CHAPTER 6

SCIENTIFIC USES OF CRUDE TELEMETRY DURING ATMOSPHERIC ENTRY

6.1 Abstract

Spacecraft entering an atmosphere often transmit information at a low data rate about their health and activities during this high-risk phase of their mission. If the spacecraft should catastrophically fail during the atmospheric entry, then this telemetry is invaluable for determining what went wrong and preventing future missions from failing in that manner. Sometimes high priority scientific data collected during the entry are also transmitted. In this Section I investigate what scientifically useful information about the atmosphere can be deduced from the basic telemetry signal. My goals are to recover some science from the mission in case of failure and verify, at a crude level, the accuracy of any atmospheric measurements made during the entry if these are later transmitted safely to Earth.

The motivation for this work comes from the failure of Mars Polar Lander, which did not return any telemetry to Earth during its atmospheric entry, and from the upcoming atmospheric entries (with telemetry) of NASA's two Mars Exploration Rovers in early 2004. I was also inspired by the problems of first measuring the surface pressure of Mars and the proposal to send very crude, expendable atmospheric probes to measure density, pressure, and temperature profiles whose results would enable the design of the first landers (Seiff, 1963). This idea was not implemented because early Mariner flybys measured the surface pressure at about the same time that earth-based observations reached a consensus. (Snyder and Moroz,

1992).

I do not analyse any data contained in the telemetry. I use only the Doppler-shifted received telemetry frequency, which depends on the speed of the spacecraft, to determine the spacecraft's trajectory and the atmosphere's properties.

In Section 6.2 I calculate the acceleration, velocity, and position of a spacecraft during atmospheric entry. In Section 6.3 I derive atmospheric properties from the spacecraft's trajectory. In Sections 6.4 –6.7 I apply my results to a hypothetical atmospheric entry to see how useful any of my techniques are in any practical applications.

6.2 Deriving Acceleration, Velocity, and Position

I first consider the dynamics of a spacecraft entering an atmosphere. For simplicity I assume a vertical entry into a non-rotating atmosphere where the only force acting on the spacecraft is aerodynamic drag:

$$\dot{z} = -v \tag{6.1}$$

$$\dot{v} = a = -\frac{\rho C_D v^2 A}{m} \tag{6.2}$$

Where z is altitude, v is speed (positive), a is $\dot{v}$ (negative), ρ is atmospheric density, C_D is the spacecraft's drag coefficient, A is the spacecraft's projected area, and m is the spacecraft's mass. An overdot indicates differentiation with respect to time. I have neglected the effects of gravity for simplicity. They are often smaller than those of drag and can easily be reintroduced into the formalism if desired. Assuming that the spacecraft's attitude is stable, C_D is a known function of the atmospheric composition (assumed known and uniform), v, ρ, and the atmospheric

temperature. Its value is usually close to 2. A and m are assumed to be known and constant during the atmospheric entry. ρ is not known. These equations are discussed in Magalhães et al. (1999).

I assume that, from analysis of the Doppler-shifted received frequency of the telemetry, v is known at equally-spaced points in time and that v changes at most linearly with t between these time points. The time interval is Δ. I label quantities corresponding to the nth time point with a subscript-n. z_0 and v_0 (at the start of the atmospheric entry) are known very accurately from spacecraft tracking during its cruise phase.

I assume that each measurement of v has the same random error, σ_v, except for v_0 which is much better known. The validity of this assumption is discussed later.

Since v changes linearly with t:

$$v\left(t\right) = v_n + \left(v_{n+1} - v_n\right) \frac{\left(t - t_n\right)}{\Delta} \tag{6.3}$$

This is valid between t_n and t_{n+1}. Using Equations 6.1 and 6.3, z_{n+1} can be found in terms of z_n:

$$z_{n+1} = z_n - \int_{t_n}^{t_{n+1}} v\left(t\right) dt \tag{6.4}$$

$$z_{n+1} = z_n - \int_{t_n}^{t_{n+1}} v_n + \left(v_{n+1} - v_n\right) \frac{\left(t - t_n\right)}{\Delta} dt \tag{6.5}$$

$$z_{n+1} = z_n - \int_{0}^{\Delta} v_n + \left(v_{n+1} - v_n\right) \frac{t}{\Delta} dt \tag{6.6}$$

$$z_{n+1} = z_n - v_n\Delta - \frac{(v_{n+1} - v_n)}{\Delta}\frac{\Delta^2}{2} \tag{6.7}$$

$$z_{n+1} = z_n - \frac{(v_{n+1} + v_n)}{2}\Delta \tag{6.8}$$

Since z_0 is known, all z_n can be found in this way.

I calculate uncertainties for all of the quantities that I derive. I use extensively the following relationship, which is valid for independent, random errors:

$$f = f(x, y, \ldots) \tag{6.9}$$

$$(\sigma_f)^2 = \left(\frac{\partial f}{\partial x}\sigma_x\right)^2 + \left(\frac{\partial f}{\partial y}\sigma_y\right)^2 + \cdots \tag{6.10}$$

The uncertainty in z_{n+1} is:

$$\sigma^2_{z_{n+1}} = \sigma^2_{z_n} + \frac{\Delta^2}{4}\left(\sigma^2_{v_{n+1}} + \sigma^2_{v_n}\right) \tag{6.11}$$

$$\sigma^2_{z_{n+1}} = \sigma^2_{z_n} + \frac{\Delta^2\sigma^2_v}{2} \tag{6.12}$$

Since $z_n - z_{n+1}$ is used later, I also use Equation 6.8 to calculate:

$$\sigma_{z_n - z_{n+1}} = \frac{\Delta\sigma_v}{2} \tag{6.13}$$

Since a is constant between time points, it must change discontinuously at each time point. This makes finding a_{n+1} challenging. I could use the average of the easily calculated a during the preceding and subsequent time intervals, but this would make a_{n+1} dependent on v_{n+2} and earlier v. This does not seem like the most appropriate way of proceeding. Instead, I look at values of a, v, and z halfway between t_n and t_{n+1}. This time is $t_{n+1/2}$. $a_{n+1/2}$, $v_{n+1/2}$, and $z_{n+1/2}$ can all be defined in terms of v_{n+1} and earlier v.

Since a is assumed constant during each Δ time interval:

$$a_{n+1/2} = \frac{v_{n+1} - v_n}{\Delta} \tag{6.14}$$

$$\sigma_{a_{n+1/2}} = \frac{\sigma_v \sqrt{2}}{\Delta} \tag{6.15}$$

And:

$$v_{n+1/2} = \frac{v_n + v_{n+1}}{2} \tag{6.16}$$

$$\sigma_{v_{n+1/2}} = \frac{\sigma_v}{\sqrt{2}} \tag{6.17}$$

$z_{n+1/2}$ is slightly more complicated to find:

$$z_{n+1/2} = z_n - \int_{t_n}^{t_{n+1/2}} v\,(t)\,dt \tag{6.18}$$

$$z_{n+1/2} = z_n - \int_{t_n}^{t_{n+1/2}} v_n + (v_{n+1} - v_n)\,\frac{(t - t_n)}{\Delta} dt \tag{6.19}$$

$$z_{n+1/2} = z_n - \int_0^{\Delta/2} v_n + (v_{n+1} - v_n)\frac{t}{\Delta} dt \tag{6.20}$$

$$z_{n+1/2} = z_n - \frac{v_n \Delta}{2} - \frac{(v_{n+1} - v_n)}{\Delta}\frac{\Delta^2}{8} \tag{6.21}$$

$$z_{n+1/2} = z_n - \frac{\Delta}{2}\frac{(3v_n + v_{n+1})}{4} \tag{6.22}$$

$$\sigma^2_{z_{n+1/2}} = \sigma^2_{z_n} + \frac{5\Delta^2\sigma_v^2}{32} \tag{6.23}$$

It is later useful to know $z_{n+3/2} - z_{n+1/2}$, so I first use Equation 6.22 to find $z_{n+3/2}$:

$$z_{n+3/2} = z_{n+1} - \frac{\Delta}{2}\frac{(3v_{n+1} + v_{n+2})}{4} \tag{6.24}$$

Using Equation 6.8:

$$z_{n+3/2} = z_n - \frac{(v_{n+1} + v_n)}{2}\Delta - \frac{\Delta}{2}\frac{(3v_{n+1} + v_{n+2})}{4} \tag{6.25}$$

$$z_{n+3/2} = z_n - \frac{3\Delta}{2}\frac{(4v_{n+1} + 4v_n + 3v_{n+1} + v_{n+2})}{12} \tag{6.26}$$

$$z_{n+3/2} = z_n - \frac{3\Delta}{2}\frac{(4v_n + 7v_{n+1} + v_{n+2})}{12} \tag{6.27}$$

Using Equation 6.22 to compare this to $z_{n+1/2}$:

$$z_{n+1/2} = z_n - \frac{3\Delta}{2}\frac{(3v_n + v_{n+1})}{12} \tag{6.28}$$

I find that:

$$z_{n+3/2} - z_{n+1/2} = \Delta\frac{(v_n + 6v_{n+1} + v_{n+2})}{8} \tag{6.29}$$

$$\sigma^2_{z_{n+3/2}-z_{n+1/2}} = \frac{\Delta^2}{64}\left(\sigma_v^2 + 36\sigma_v^2 + \sigma_v^2\right) \tag{6.30}$$

$$\sigma^2_{z_{n+3/2}-z_{n+1/2}} = \frac{\Delta^2}{32}\left(19\sigma_v^2\right) \tag{6.31}$$

6.3 Deriving Atmospheric Properties

Useful atmospheric properties that can be obtained from these data include vertical profiles of density, pressure, and temperature. There is more than one way to calculate atmospheric properties from measurements of v. Different techniques involve different approximations. An approximate technique may be better than a formally correct technique if the uncertainty on the formally correct estimate of, say, temperature is many times greater than that on the approximate estimate. I shall outline several techniques and then investigate which of them are most useful.

I shall outline one technique for deriving atmospheric density, three techniques for atmospheric pressure, and four for atmospheric temperature. I shall use a variety of superscripts to distinguish pressures and temperatures derived by different techniques. All uncertainty calculations are discussed in Appendix F.

6.3.1 First Technique for Density

Rearranging Equation 6.2, I find that:

$$\rho = \frac{-a}{v^2}\frac{m}{C_D A} \tag{6.32}$$

If C_D is known, then Equation 6.32 can be solved to give the value of ρ at each $t_{n+1/2}$. Since z is also known at these times from Equation 6.22, I have ρ as a function of z.

$$\rho_{n+1/2} = \frac{-a_{n+1/2}}{v_{n+1/2}^2}\frac{m}{C_D A} \tag{6.33}$$

Using Equations 6.14 and 6.16:

$$\rho_{n+1/2} = \frac{v_{n+1} - v_n}{\left(v_n + v_{n+1}\right)^2}\frac{4m}{\Delta A C_D} \tag{6.34}$$

6.3.2 First Technique for Pressure

In the usual manner, this density profile can be converted into a pressure profile using hydrostatic equilibrium. A temperature profile can then be obtained using an equation of state and the density and pressure profiles. To distinguish the results of this technique from later ones, I label pressures calculated using this technique by p^*.

$$p = \int -\rho g dz \tag{6.35}$$

Where p is pressure and g is the planet's acceleration due to gravity. Rather than using a complicated upper boundary condition, I set p_0 equal to zero. This does not affect results in the lower atmosphere and, as I shall show later, uncertainties in the upper atmosphere are large enough that they prevent any useful estimate of p_0 from the density scale height.

$$p^*_{n+1} = p^*_n + \rho_{n+1/2} g \left(z_n - z_{n+1}\right) \tag{6.36}$$

$\rho_{n+1/2}$ can be calculated from Equation 6.34 and $z_n - z_{n+1}$ can be calculated from Equation 6.8.

6.3.3 First Technique for Temperature

To distinguish the results of this technique from later ones, I label temperatures calculated using this technique by T^*. Atmospheric temperature is given by the ideal gas equation of state:

$$T = \frac{p M_{mol}}{\rho k_B} \tag{6.37}$$

Where M_{mol} is the mean molecular mass of the atmosphere (assumed known), and k_B is Boltzmann's constant. Unfortunately, I have calculated above p^*_n and $\rho_{n+1/2}$. A reasonable estimate for ρ_n is the geometric mean of $\rho_{n-1/2}$ and $\rho_{n+1/2}$:

$$\rho^2_n = \rho_{n-1/2} \rho_{n+1/2} \tag{6.38}$$

$\rho_{n-1/2}$ and $\rho_{n+1/2}$ can be calculated from Equation 6.34. This is correct in the case when v stays constant between $t_{n-1/2}$ and $t_{n+1/2}$ and the atmosphere is isothermal between $z_{n-1/2}$ and $z_{n+1/2}$.

$$T_n^* = \frac{M_{mol}}{k_B}\frac{p_n^*}{\rho_n} \tag{6.39}$$

p_n^* can be calculated from Equation 6.36 and ρ_n can be calculated from Equation 6.38.

6.3.4 Second Technique for Temperature

Another technique can also be used. I label temperatures calculated using this technique by $T^{@}$ to distinguish them from those of Section 6.3.3. For an isothermal atmosphere in hydrostatic equilibrium, $\rho(z)$ can be related to atmospheric temperature, T:

$$T = \frac{-M_{mol}g}{k_B}\frac{dz}{d\ln\rho} \tag{6.40}$$

$$T_n^{@} = \frac{-M_{mol}g}{k_B}\frac{z_{n+1/2} - z_{n-1/2}}{\ln\rho_{n+1/2} - \ln\rho_{n-1/2}} \tag{6.41}$$

$$T_n^{@} = \frac{-M_{mol}g}{k_B}\frac{z_{n+1/2} - z_{n-1/2}}{\ln\left(\frac{\rho_{n+1/2}}{\rho_{n-1/2}}\right)} \tag{6.42}$$

Using Equation 6.29:

$$T_n^{@} = \frac{M_{mol}g}{8k_B}\Delta\frac{(v_{n-1} + 6v_n + v_{n+1})}{\ln\left(\frac{\rho_{n+1/2}}{\rho_{n-1/2}}\right)} \tag{6.43}$$

As long as C_D does not change significantly between $t_{n-1/2}$ and $t_{n+1/2}$, the ratio of densities can be calculated without it. Using Equation 6.34:

$$\frac{\rho_{n+1/2}}{\rho_{n-1/2}} = \frac{v_{n+1} - v_n}{(v_n + v_{n+1})^2} \frac{(v_{n-1} + v_n)^2}{v_n - v_{n-1}} \tag{6.44}$$

$$T_n^{@} = \frac{M_{mol} g}{8 k_B} \Delta \frac{(v_{n-1} + 6v_n + v_{n+1})}{\ln\left(\frac{v_{n+1}-v_n}{(v_n+v_{n+1})^2} \frac{(v_{n-1}+v_n)^2}{v_n - v_{n-1}}\right)} \tag{6.45}$$

6.3.5 Second Technique for Pressure

I label pressures calculated in this section as $p^{@}$. To find the pressure from the density and temperature, I use the ideal gas equation of state and ρ_n from Equation 6.38:

$$p_n^{@} = \rho_n T_n^{@} \frac{k_B}{M_{mol}} \tag{6.46}$$

$T_n^{@}$ can be calculated using Equation 6.45 and ρ_n can be calculated from Equation 6.38.

6.3.6 Third Technique for Temperature

If the acceleration is constant between three, not just two, time points, then Equation 6.45 for $T_n^{@}$ can be simplified. I label this calculation of T as $T^{\#}$. Using $v_{n-1} = v_n + \delta$ and $v_{n+1} = v_n - \delta$, Equation 6.45 gives:

$$T_n^{\#} = \frac{M_{mol} g}{8 k_B} \Delta \frac{8 v_n}{\ln\left(\frac{-\delta}{(2v_n-\delta)^2} \frac{(2v_n+\delta)^2}{-\delta}\right)} \tag{6.47}$$

$$T_n^{\#} = \frac{M_{mol}g}{k_B}\Delta\frac{v_n}{2\ln\left(\frac{1+\delta/2v_n}{1-\delta/2v_n}\right)} \tag{6.48}$$

$$T_n^{\#} = \frac{M_{mol}g}{k_B}\Delta\frac{v_n}{2\ln\left(1+\delta/v_n\right)} \tag{6.49}$$

$$T_n^{\#} = \frac{M_{mol}g}{k_B}\Delta\frac{v_n^2}{2\delta} \tag{6.50}$$

$$T_n^{\#} = \frac{M_{mol}g\Delta}{k_B}\frac{v_n^2}{v_{n-1}-v_{n+1}} \tag{6.51}$$

Uncertainties for this derivation of temperature are small, but there are only restricted circumstances in which it can be used.

6.3.7 Third Technique for Pressure

There is yet another approach to finding atmospheric properties. v and z are better known than a, since a involves taking the difference of two large, inaccurate numbers. I label pressures calculated by this technique $p^{\#}$. Dividing Equation 6.1 by Equation 6.2 gives:

$$\frac{dv}{dz} = \frac{\rho C_D A v}{m} \tag{6.52}$$

$$\int\frac{dv}{v} = \int\frac{\rho g C_D A}{mg}dz \tag{6.53}$$

If I assume that C_D is constant, then by hydrostatic equilibrium:

$$\int \frac{dv}{v} = \frac{-C_D A}{mg} \int dp^{\#} \tag{6.54}$$

$$\ln\left(\frac{v_n}{v_x}\right) = \frac{-C_D A}{mg}\left(p_n^{\#} - p_x\right) \tag{6.55}$$

$$\left(p_n^{\#} - p_x\right) = \frac{-mg}{C_D A} \ln\left(\frac{v_n}{v_x}\right) \tag{6.56}$$

This formula for p, unlike Equation 6.34 for ρ, does not depend on the difference between two velocities. p_x is unknown, but if I use the top of the atmosphere as a boundary condition, where $v_x = v_0$ is known accurately and p_x is small, then its actual value is irrelevant for values of p lower in the atmosphere.

6.3.8 Fourth Technique for Temperature

I label temperatures calculated by this technique $T^{\$}$. Similarly to before, assuming an isothermal atmosphere gives:

$$T^{\$} = \frac{-M_{mol} g}{k_B} \frac{dz}{d\left(\ln p^{\#}\right)} \tag{6.57}$$

$$T^{\$}_{n+1/2} = \frac{M_{mol} g}{k_B} \frac{z_n - z_{n+1}}{\ln p^{\#}_{n+1} - \ln p^{\#}_n} \tag{6.58}$$

Using Equation 6.8:

$$T^{\$}_{n+1/2} = \frac{M_{mol} g \Delta}{2 k_B} \frac{v_n + v_{n+1}}{\ln\left(\frac{p^{\#}_{n+1}}{p^{\#}_{n}}\right)} \tag{6.59}$$

$p^{\#}_n$ can be calculated from Equation 6.56.

6.3.9 Summary

The techniques in Sections 6.3.1 – 6.3.6 are closely related to the traditional method of entry accelerometer data analysis practised by Seiff and colleagues. I have not come across the techniques in Sections 6.3.7 – 6.3.8 in the literature of this discipline. Treating C_D as constant is a source of error that I have not considered in the formal uncertainty analysis. Figure 3 of Magalhães et al. (1999) shows how C_D changed during Pathfinder's descent. However, if there are other large sources of error, this incorrect assumption may be justified. C_D changes by at most 25% over the entire descent of Pathfinder, so densities derived with this assumption are only incorrect by 25% due to this assumption. With changes in density of 8 orders of magnitude, that is not necessarily a major problem. Pressures are in error by a similar amount. The error in density is due to errors in C_D at that instant. However, the errors in pressure are proportional to accumulated errors in C_D over the previous 2 scale heights or so. Densities are directly proportional to C_D, so estimates of the ratio of two densities are not affected by this error as long as C_D does not change greatly between the two points of interest. Estimates of the ratio of two pressures are similarly robust, as are temperatures estimated from the ratio of a pressure and a density measurement.

6.4 Uncertainties in Transmitted Frequency

In the special case in which the line of sight between spacecraft and receiver is parallel to the vertical trajectory of the spacecraft, v is related to the received and

transmitted frequencies as follows:

$$\frac{v}{c} = \frac{f_{trans} - f_{rec}}{f_{trans}} = 1 - \frac{f_{rec}}{f_{trans}} \tag{6.60}$$

$$c - v = c\frac{f_{rec}}{f_{trans}} \tag{6.61}$$

Where c is the speed of light, f_{trans} is the transmitted frequency and f_{rec} is the received frequency. c is known exactly, and f_{rec} is known much more accurately than f_{trans}.

$$\frac{\sigma_{c-v}}{c - v} = \frac{\sigma_{f_{trans}}}{f_{trans}} \tag{6.62}$$

$$\sigma_{c-v} = \sigma_v = (c - v)\frac{\sigma_{f_{trans}}}{f_{trans}} \tag{6.63}$$

$$\sigma_v = c\frac{f_{rec}}{f_{trans}}\frac{\sigma_{f_{trans}}}{f_{trans}} \tag{6.64}$$

Since $v \ll c$ in Equation 6.61:

$$\sigma_v = c\frac{\sigma_{f_{trans}}}{f_{trans}} \tag{6.65}$$

Sam Thurman of JPL has also considered this problem. He sent me some information on the uncertainties in transmitted frequency for Mars Pathfinder (personal communication, 2002). The nominal transmission frequency was about 8.4

GHz. The free-fall drift rate of the oscillator, measured prior to entry, was a few tenths of Hz per second. Extrapolated through the three hundred second atmospheric entry this causes a frequency drift of about 100 Hz. The oscillator frequency is very sensitive to acceleration. Thurman modelled this as a quadratic in g with coefficients of 10 Hz g^{-1} and 5 Hz g^{-2}. In the worst case in which these two terms both cause frequency shifts in the same direction, this effect causes a frequency shift of 600 Hz at maximum acceleration of 10 g. Random noise levels prior to parachute opening were modelled as 3 Hz. This increased to 50 Hz after parachute opening. Parachute opening caused an instantaneous 250 Hz shift in frequency. In this work I am only interested in behaviour prior to parachute opening and find it simplest to model $\sigma_{f_{trans}}$ as random noise. I use $\sigma_{f_{trans}}/f_{trans} = 10^{-7}$. This is slightly larger than Thurman's modelling of the systematic drift which dominates $\sigma_{f_{trans}}$. Assuming that $\sigma_{f_{trans}}$ is random noise allows me to use the equations above. If I assumed a systematic drift, then a more complicated treatment of the errors would be needed.

6.5 Simulated Trajectory and Atmospheric Properties

To see how useful all of this is, I need to use some realistic numbers. I chose those of Mars Pathfinder: $m = 500$ kg and $A = 5$ m^2. The martian atmosphere has $M_{mol} = 44 \times 1.67 \times 10^{-27}$ kg and $g = 3.7$ m s^{-2}. Of course, $k_B = 1.38 \times 10^{-23}$ J K^{-1}.

I use a vertical atmospheric entry from 120 km altitude to the surface. For simplicity I allow my spacecraft to impact the surface at high speed without braking with parachutes or rockets. I assume a vertical entry speed of 2 km s^{-1}, which is the same as Pathfinder's vertical component of velocity. Pathfinder's actual speed was faster, but on a shallower flight path. I assume that $C_D = 2$ under all conditions. The atmosphere is isothermal at 200 K, with a surface density of 10^{-2} kg m^{-3} and a scale height of 10 km.

I first calculate v, z, a, ρ, p, and T that are actually experienced during

the simulated descent as functions of t. a is known from Equation 6.2, v from integrating Equation 6.2, and z from integrating Equation 6.1. I use a simple first-order integration routine with a timestep of 1 s. Using shorter timesteps did not change the derived trajectory. T is always 200 K. ρ is found from integrating Equation 6.40 and p is found from Equation 6.37. z, v, a, ρ, and p are plotted as functions of t in Figures 6.1 – 6.5.

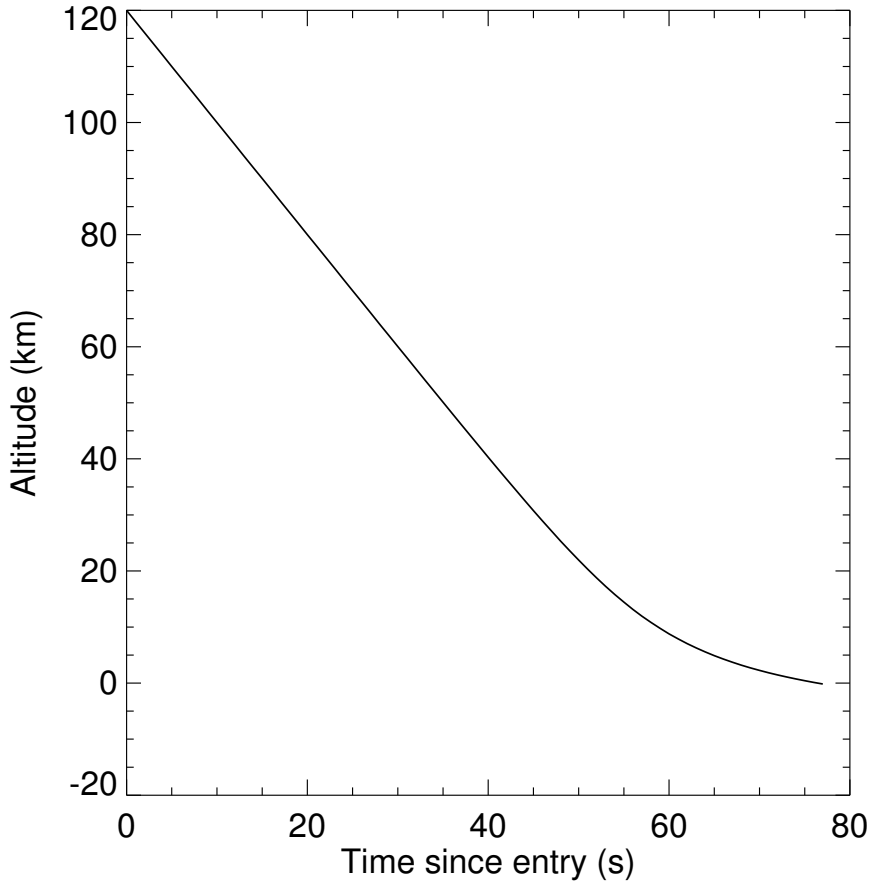

Figure 6.1: Altitude versus time for the simulated atmospheric entry

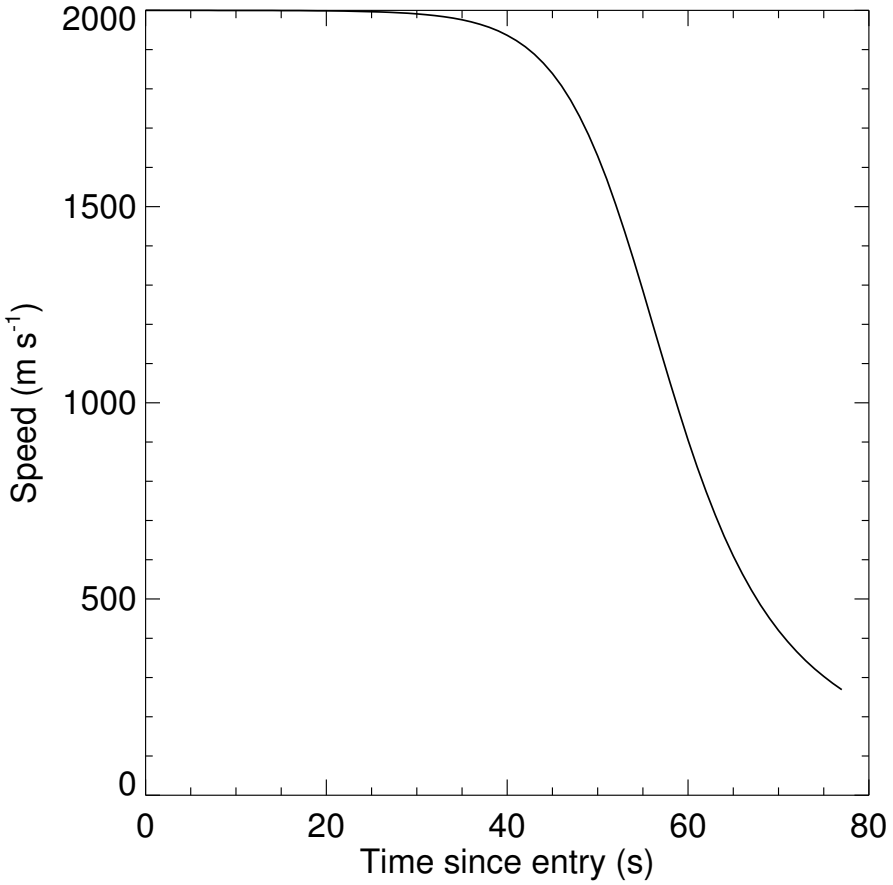

Figure 6.2: Speed versus time for the simulated atmospheric entry

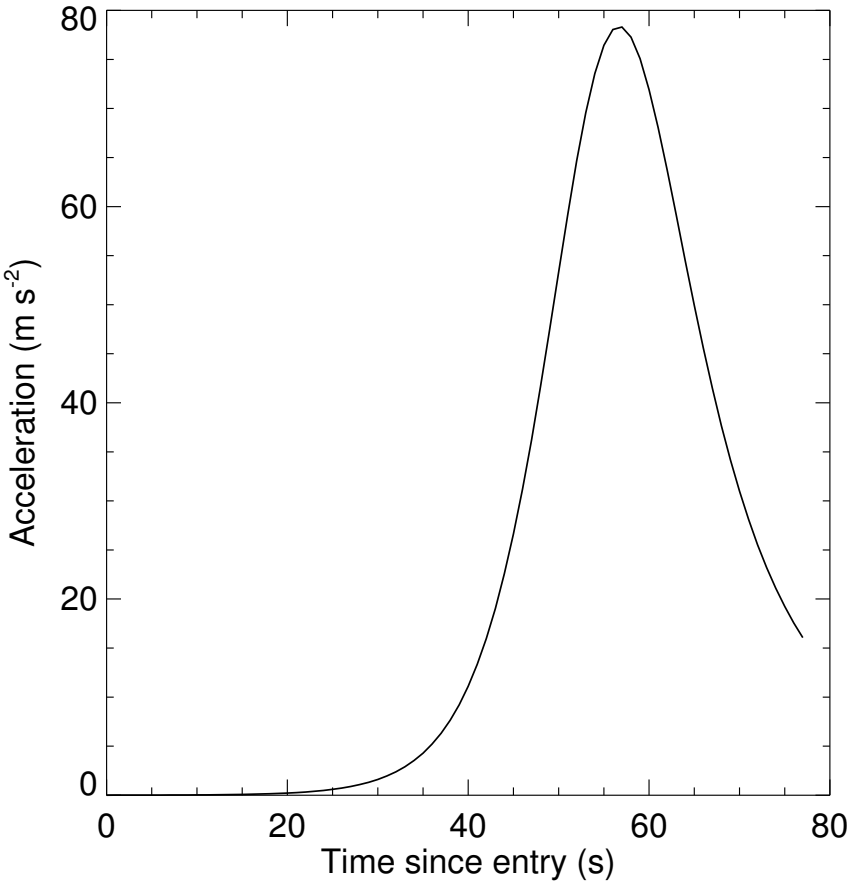

Figure 6.3: Acceleration versus time for the simulated atmospheric entry

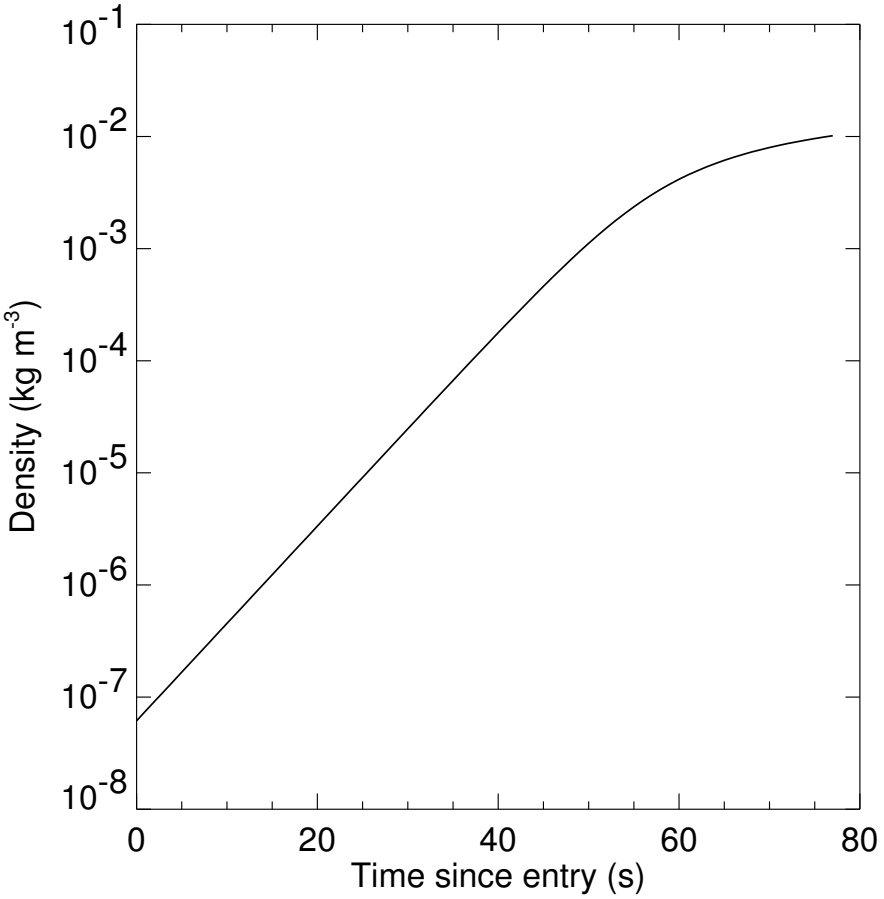

Figure 6.4: Density versus time for the simulated atmospheric entry

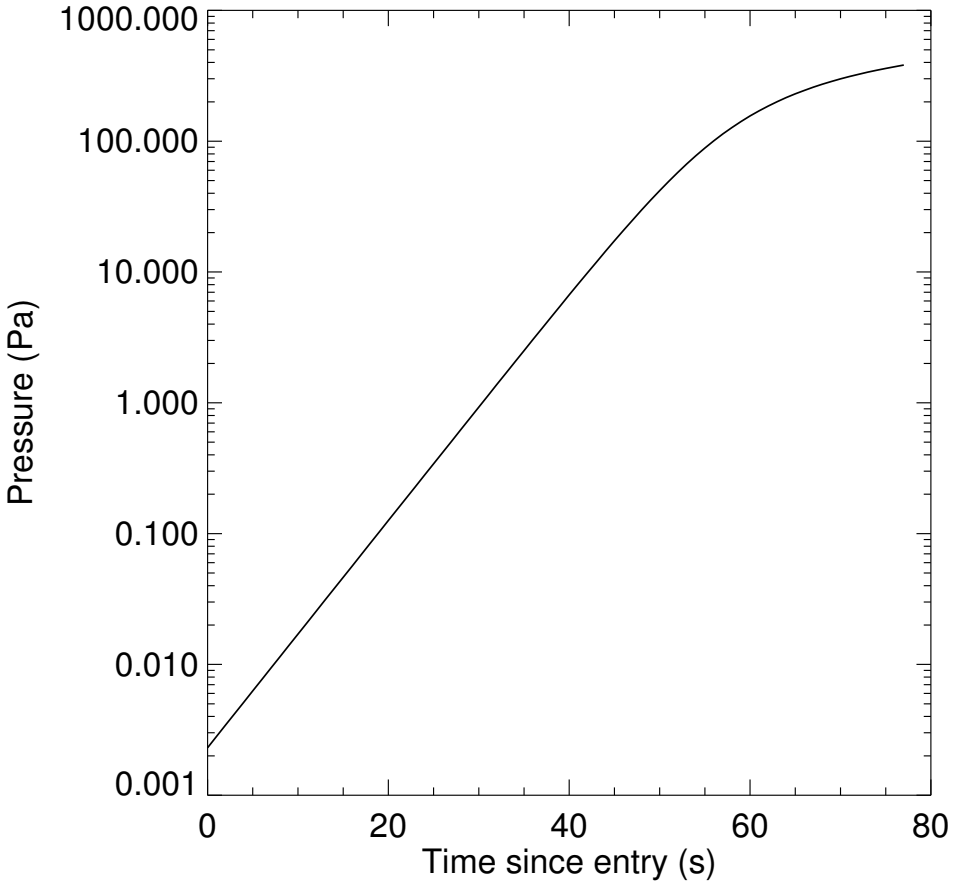

Figure 6.5: Pressure versus time for the simulated atmospheric entry

The total flight time is about 70 – 80 seconds. This is much shorter than Pathfinder's 300 s descent because of Pathfinder's shallower flight path. I chose Δ to be 4 s. In reality telemetry is continuous, not intermittent. In that case signals within a certain time interval are averaged to reduce their random noise level. The time interval should be long enough to usefully reduce the noise and short enough that atmospheric properties are not changing too much during it. Since I am representing a systematic drift as a random noise in order to get an idea for what's going on, I cannot average to reduce the noise level. 4 s at 2 km s^{-1} corresponds to travelling nearly an atmospheric scale height.

6.6 Derived Trajectory and Atmospheric Properties Using Clean v

First, I calculated z, v, a, ρ, p, and T from my various techniques using the simulated values of v with the specified σ_v of $c/10^7$. With this approach, calculated quantities should be close to their simulated values and the uncertainties should be somewhat realistic. Afterwards I use noisy values of v to calculate all these quantities.

Figures 6.6 – 6.19 show z_n, $z_{n+1/2}$, v_n, $v_{n+1/2}$, $a_{n+1/2}$, $\rho_{n+1/2}$, ρ_n, p_n^*, $p_n^@$, $p_n^\#$, T_n^*, $T_n^@$, $T_n^\#$, and $T_{n+1/2}^\$$ as functions of t. Uncertainties for each quantitity are plotted, as are the simulated values experienced during entry.

Both z_n and $z_{n+1/2}$ (Figures 6.6 and 6.7) have uncertainties smaller than the size of the symbols. $v_{n+1/2}$ (Figure 6.9) has uncertainties smaller than the size of the symbols. $a_{n+1/2}$ (Figure 6.10) has large uncertainties. This suggests that quantities derived from $a_{n+1/2}$ are uncertain. $\rho_{n+1/2}$ (Figure 6.11) only has small uncertainties after $t = 40$ s. ρ_n (Figure 6.12) only has small uncertainties between $t = 45$ s and 70 s. p_n^* (Figure 6.13) only has small uncertainties after $t = 40$ s. $p_n^@$ (Figure 6.14) never has small uncertainties. $p_n^\#$ (Figure 6.15) only has small uncertainties after $t = 40$ s. T_n^* (Figure 6.16) only has uncertainties of less than 100 K between $t = 50$ s and 60 s. $T_n^@$ (Figure 6.17) is similar. $T_n^\#$ (Figure 6.18) is interesting. This temperature measurement is only valid when a is constant during two consecutive

time intervals. This corresponds to the peak in Figure 6.10. If this peak can be accurately located in the data, then *one* good temperature measurement with small uncertainties can be made. In this case, it is at about $t = 55$ s. Using simulated (not noisy) v gives a very good measurement of the temperature at this point. I shall later investigate how good the measurement is using noisy v data. $T^{\$}_{n+1/2}$ (Figure 6.19) has uncertainties of less than 100 K after $t = 40$ s.

p^{*}_{n} and $p^{\#}_{n}$ have smaller uncertainties than $p^{@}_{n}$. $T^{\$}_{n+1/2}$ has smaller uncertainties than T^{*}_{n} and $T^{@}_{n}$. $T^{\#}_{n}$ may give one and only one accurate temperature measurement during descent at the time of maximum acceleration.

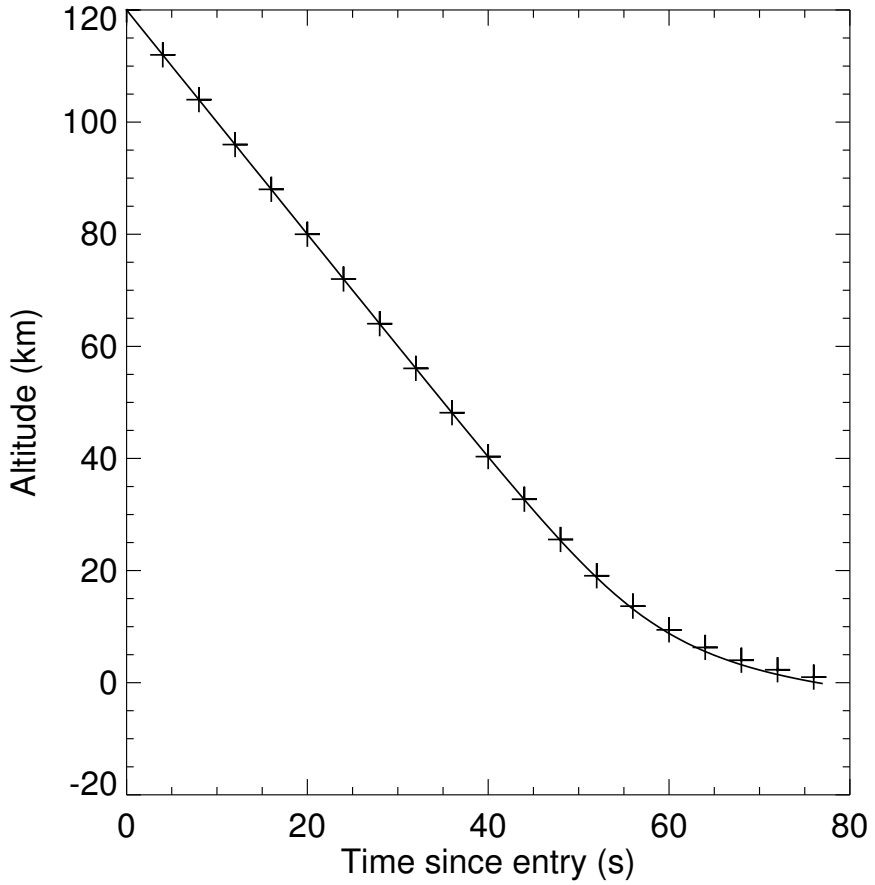

Figure 6.6: z_n (crosses) and σ_{z_n} (vertical lines) versus time calculated using simulated v. Continuous curve is simulated z versus t experienced during the atmospheric entry.

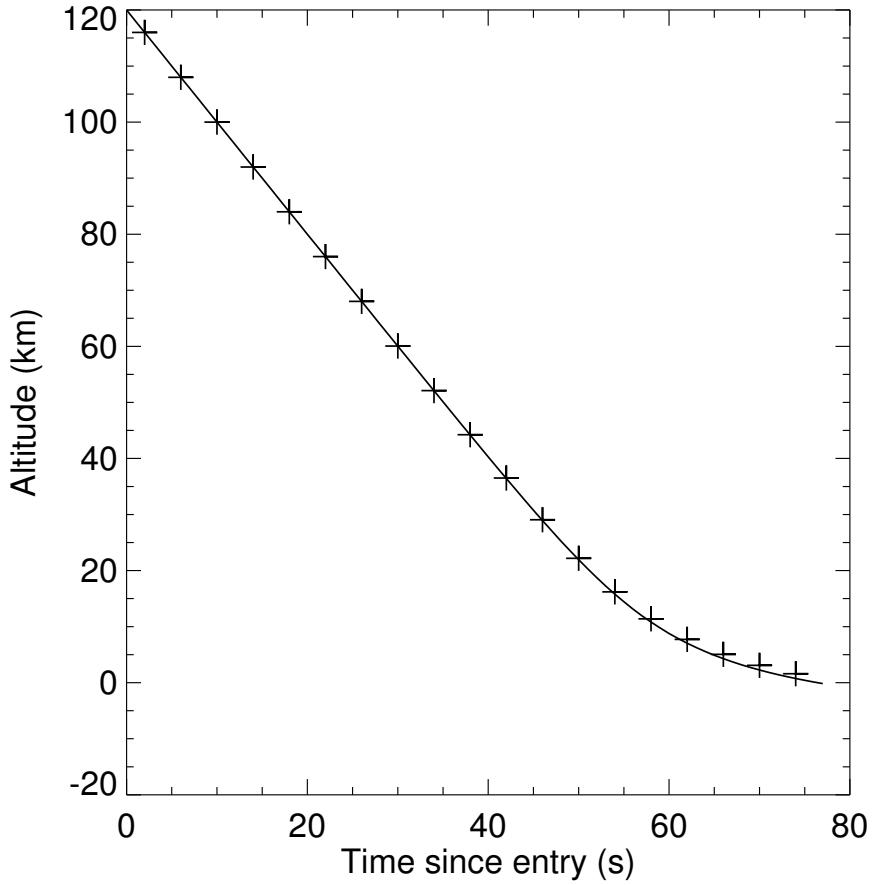

Figure 6.7: $z_{n+1/2}$ (crosses) and $\sigma_{z_{n+1/2}}$ (vertical lines) versus time calculated using simulated v. Continuous curve is simulated z versus t experienced during the atmospheric entry.

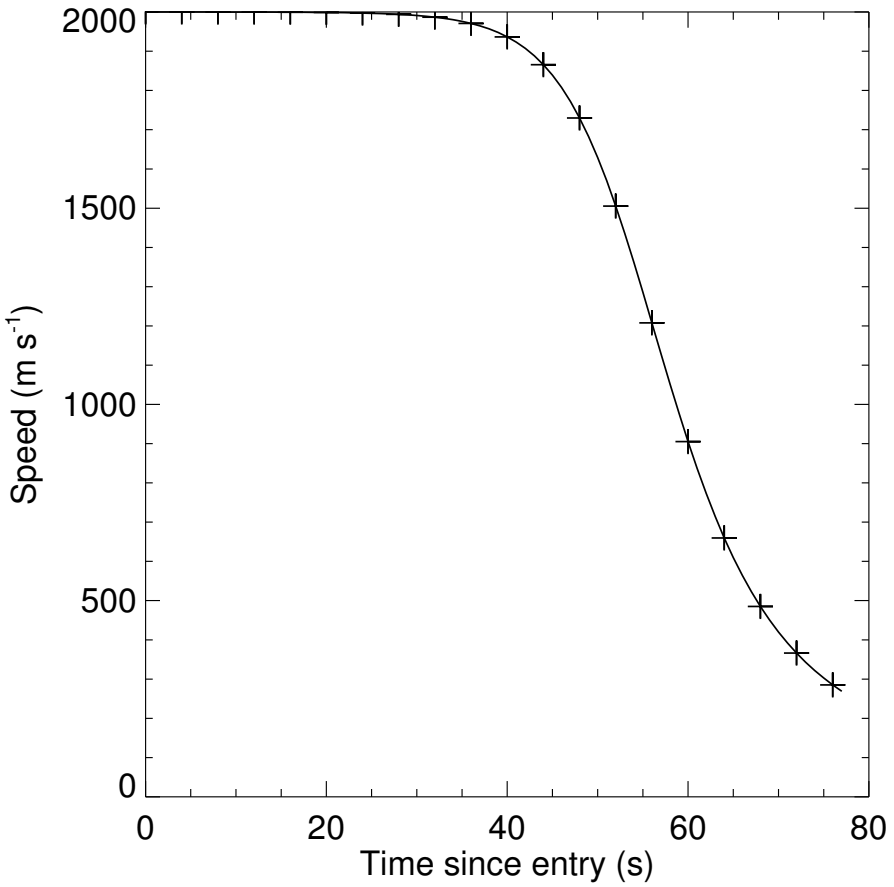

Figure 6.8: v_n (crosses) and σ_{v_n} (vertical lines) versus time calculated using simulated v. Continuous curve is simulated v versus t experienced during the atmospheric entry.

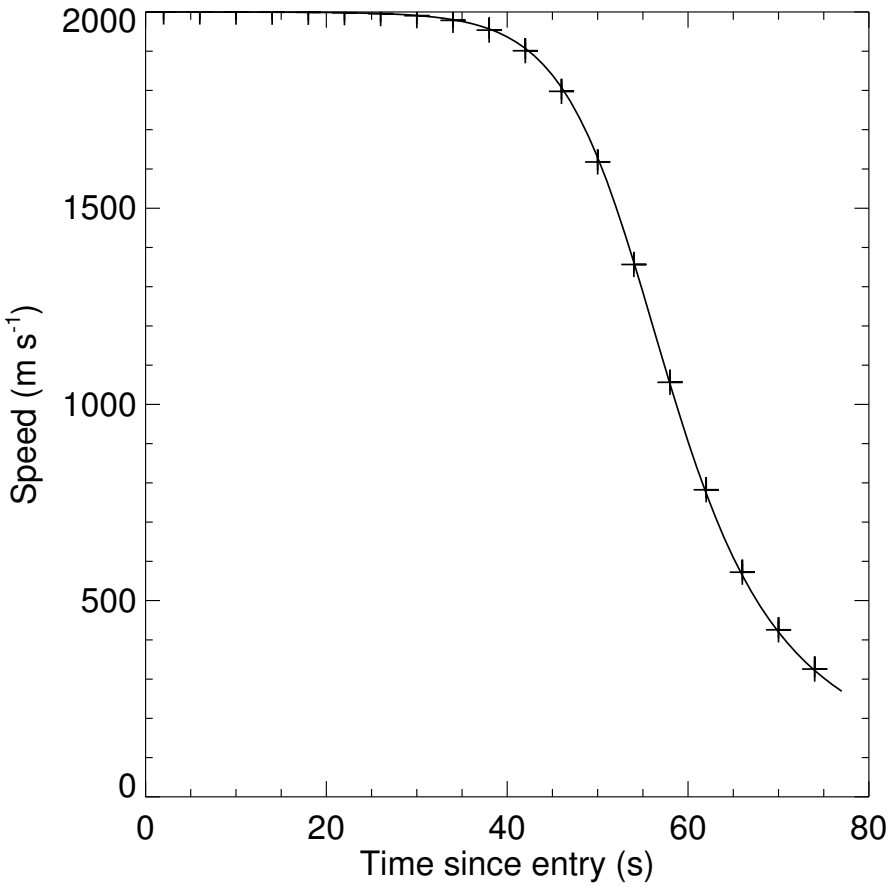

Figure 6.9: $v_{n+1/2}$ (crosses) and $\sigma_{v_{n+1/2}}$ (vertical lines) versus time calculated using simulated v. Continuous curve is simulated v versus t experienced during the atmospheric entry.

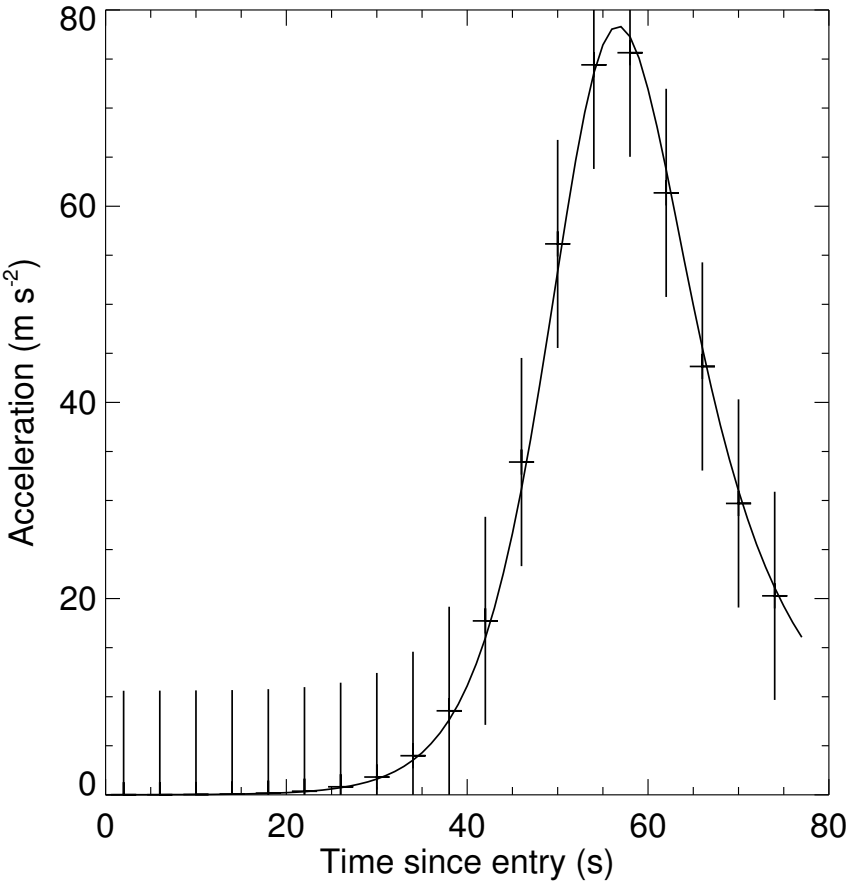

Figure 6.10: $a_{n+1/2}$ (crosses) and $\sigma_{a_{n+1/2}}$ (vertical lines) versus time calculated using simulated v. Continuous curve is simulated a versus t experienced during the atmospheric entry.

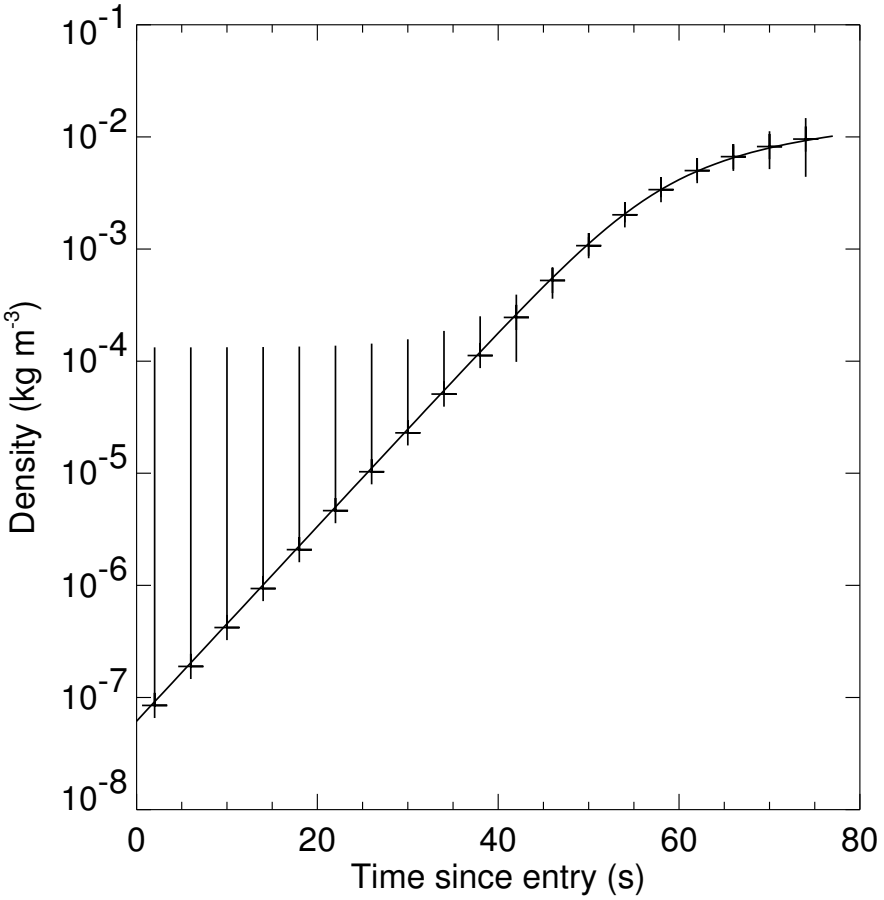

Figure 6.11: $\rho_{n+1/2}$ (crosses) and $\sigma_{\rho_{n+1/2}}$ (vertical lines) versus time calculated using simulated v. If $\rho_{n+1/2} - \sigma_{\rho_{n+1/2}}$ is negative, then only one side of the error bar is plotted. Continuous curve is simulated ρ versus t experienced during the atmospheric entry.

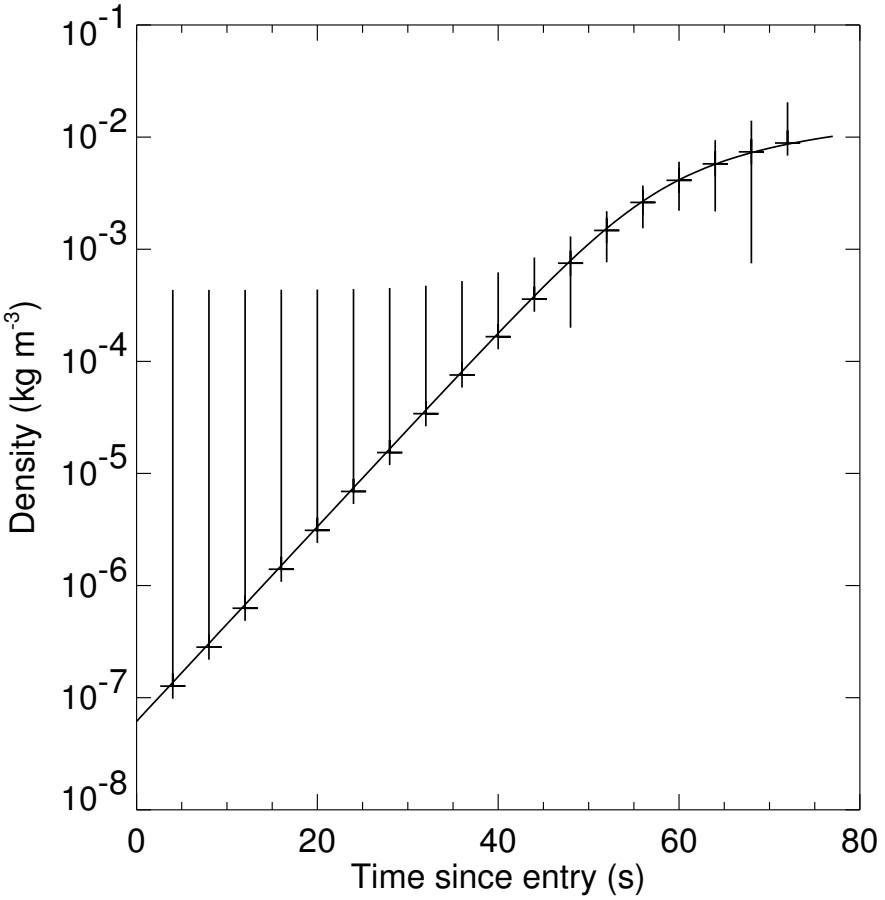

Figure 6.12: ρ_n (crosses) and σ_{ρ_n} (vertical lines) versus time calculated using simulated v. If $\rho_n - \sigma_{\rho_n}$ is negative, then only one side of the error bar is plotted. Continuous curve is simulated ρ versus t experienced during the atmospheric entry.

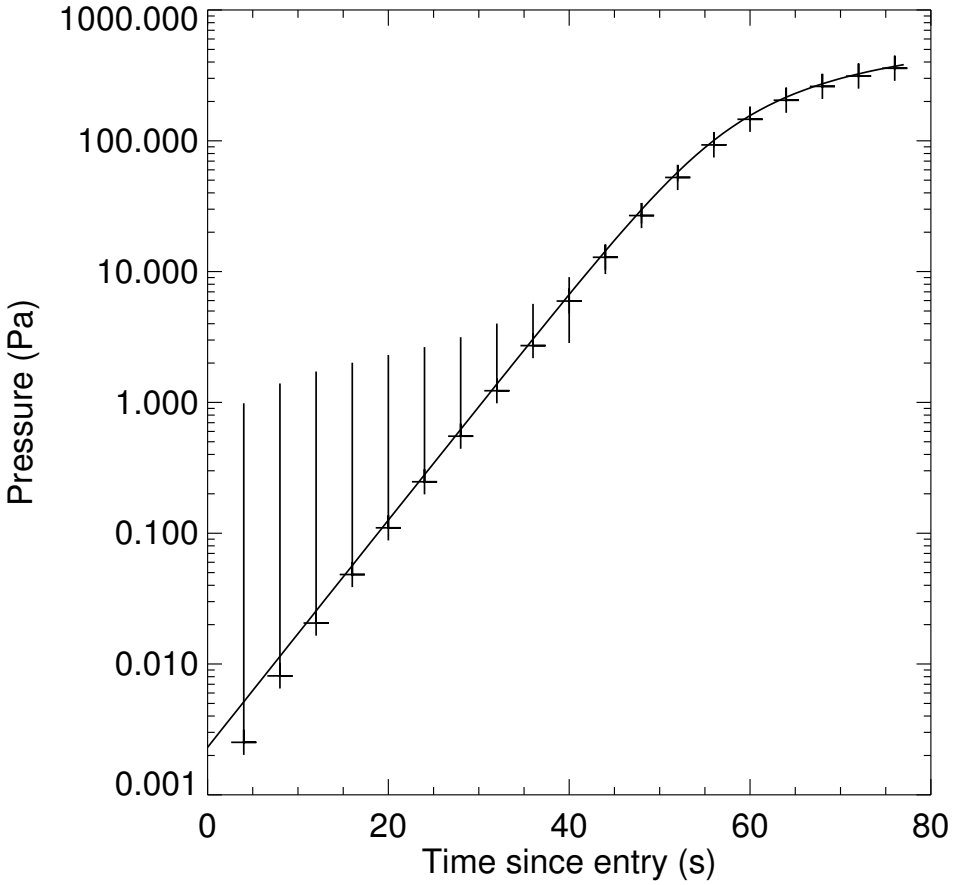

Figure 6.13: p_n^* (crosses) and $\sigma_{p_n^*}$ (vertical lines) versus time calculated using simulated v. If $p_n^* - \sigma_{p_n^*}$ is negative, then only one side of the error bar is plotted. Continuous curve is simulated p versus t experienced during the atmospheric entry.

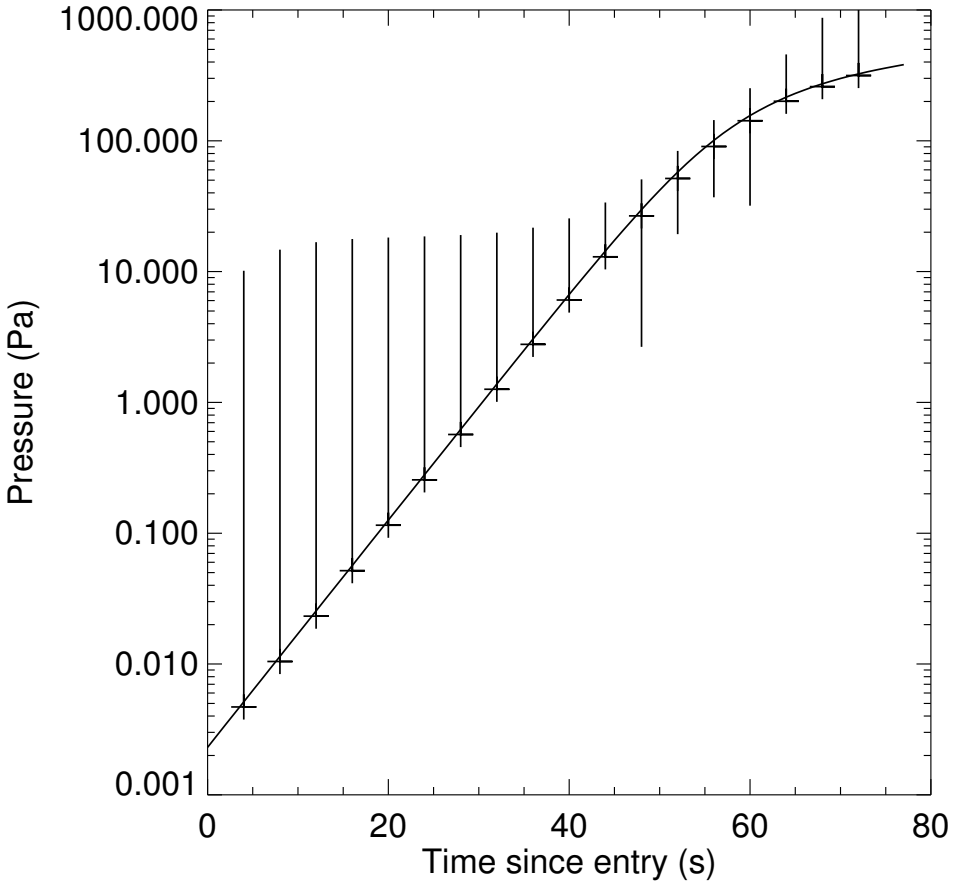

Figure 6.14: $p_n^{@}$ (crosses) and $\sigma_{p_n^{@}}$ (vertical lines) versus time calculated using simulated v. If $p_n^{@} - \sigma_{p_n^{@}}$ is negative, then only one side of the error bar is plotted. Continuous curve is simulated p versus t experienced during the atmospheric entry.

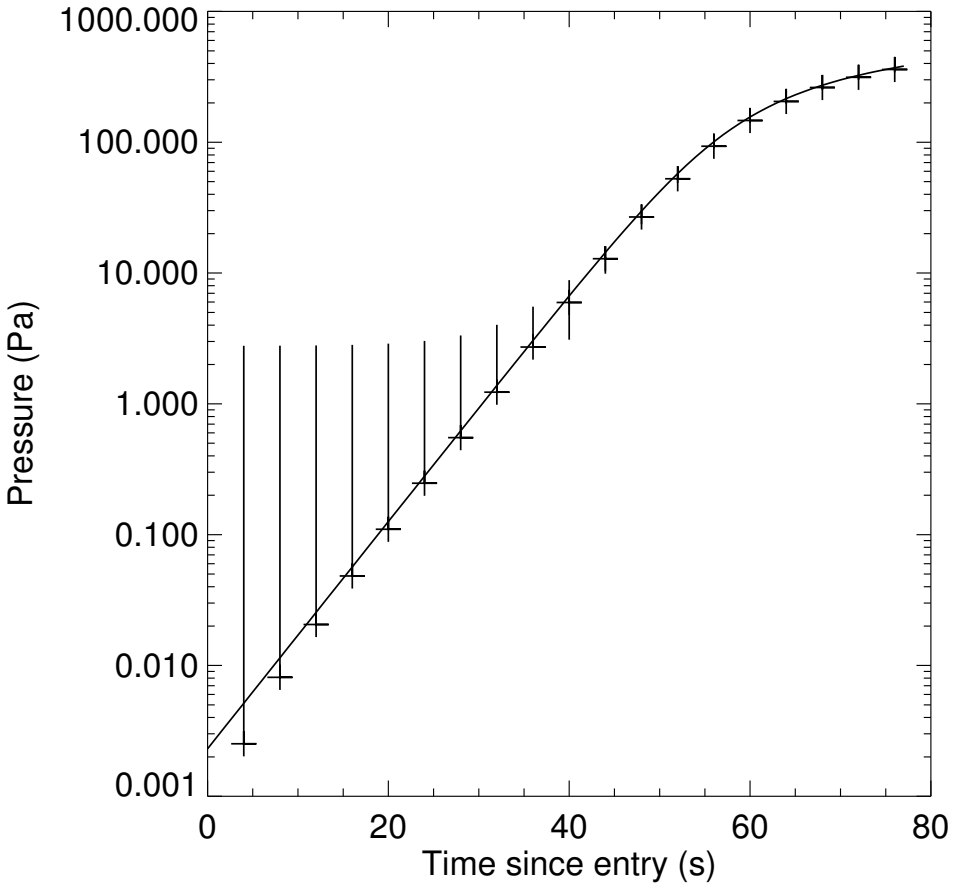

Figure 6.15: $p_n^{\#}$ (crosses) and $\sigma_{p_n^{\#}}$ (vertical lines) versus time calculated using simulated v. If $p_n^{\#} - \sigma_{p_n^{\#}}$ is negative, then only one side of the error bar is plotted. Continuous curve is simulated p versus t experienced during the atmospheric entry.

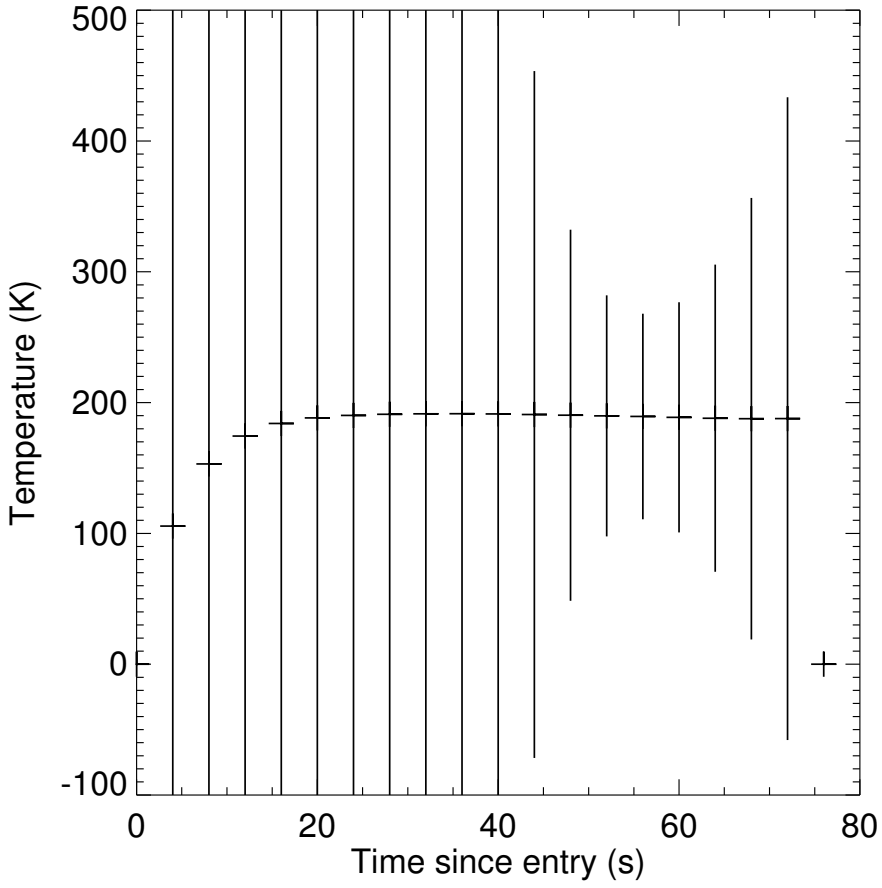

Figure 6.16: T_n^* (crosses) and $\sigma_{T_n^*}$ (vertical lines) versus time calculated using simulated v. Simulated T during the atmospheric entry is 200 K.

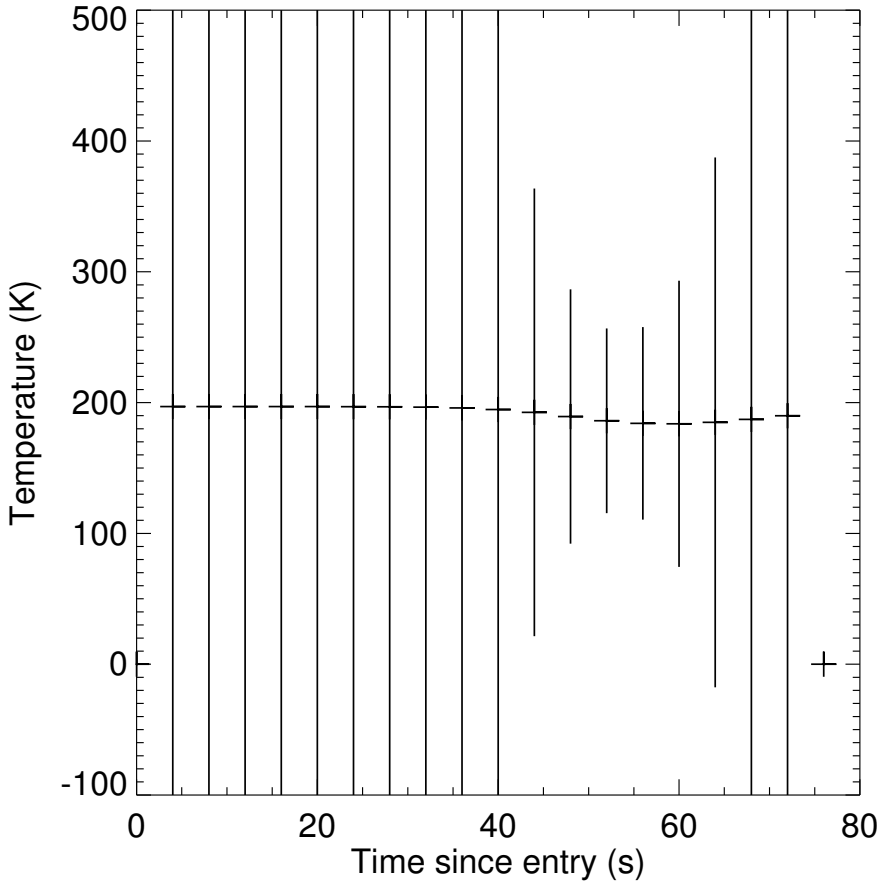

Figure 6.17: $T_n^{@}$ (crosses) and $\sigma_{T_n^{@}}$ (vertical lines) versus time calculated using simulated v. Simulated T during the atmospheric entry is 200 K.

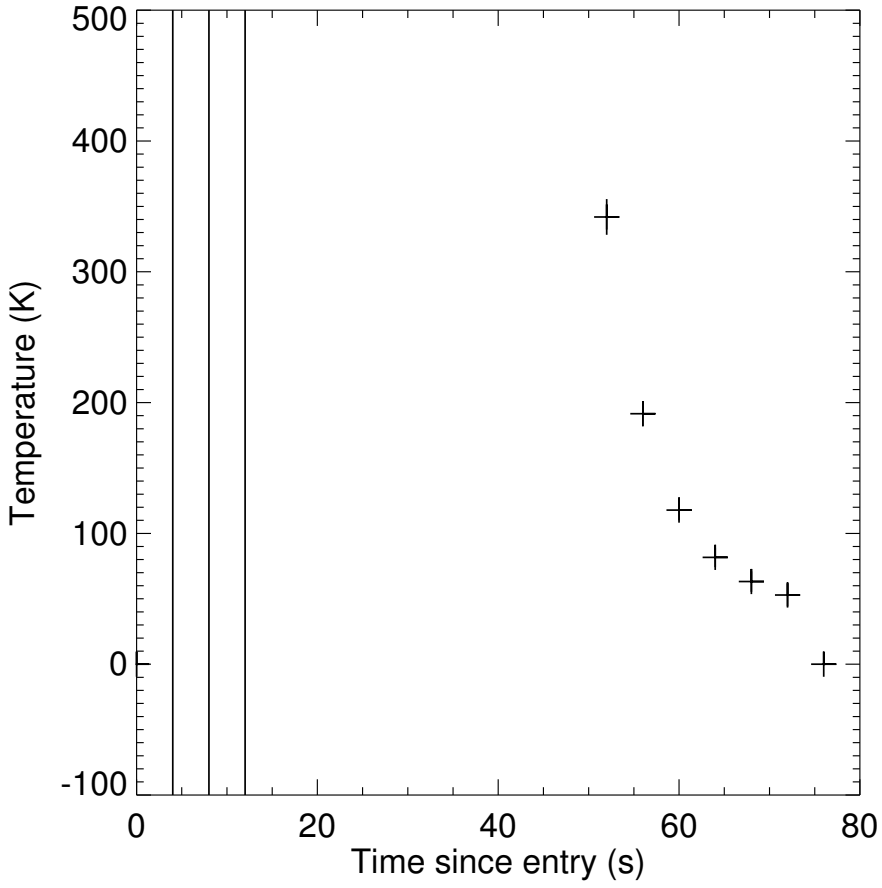

Figure 6.18: $T_n^{\#}$ (crosses) and $\sigma_{T_n^{\#}}$ (vertical lines) versus time calculated using simulated v. Simulated T during the atmospheric entry is 200 K.

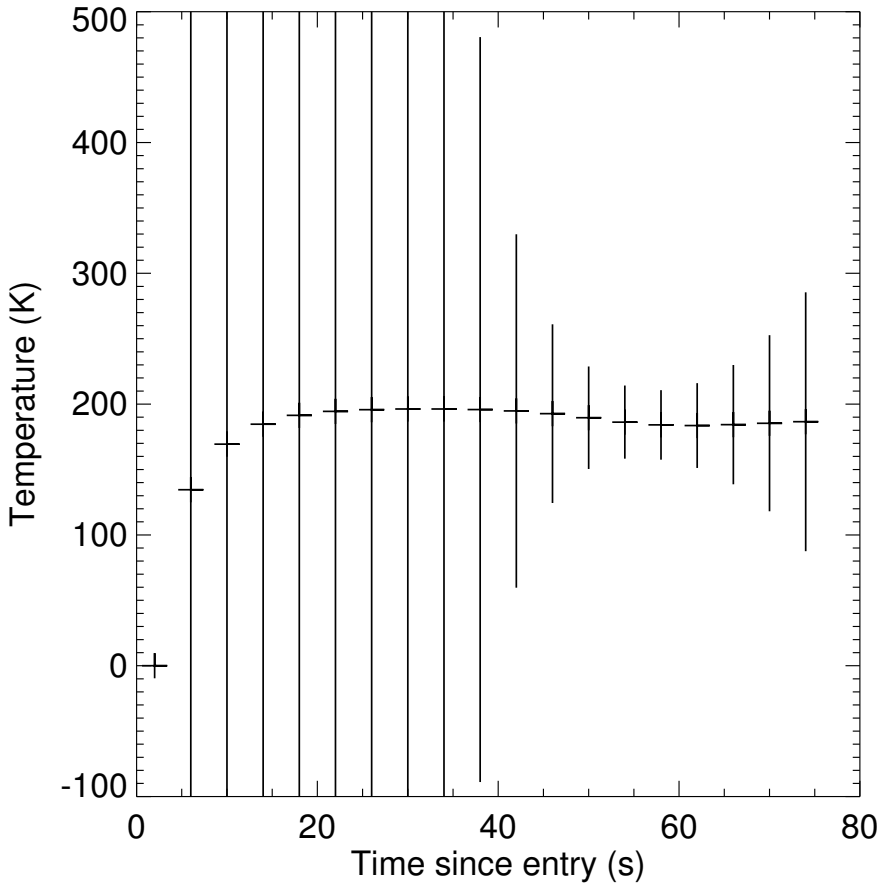

Figure 6.19: $T^{\$}_{n+1/2}$ (crosses) and $\sigma_{T^{\$}_{n+1/2}}$ (vertical lines) versus time calculated using simulated v. Simulated T during the atmospheric entry is 200 K.

6.7 Derived Trajectory and Atmospheric Properties Using Noisy v

Next I added random noise corresponding to σ_v to the v_n derived at each time point from the telemetry. I used the noisy v_n and σ_v to calculate z, v, a, ρ, p, and T from my various techniques. This is the closest analogy to actual practical application of these techniques on real data.

Figures 6.20 – 6.33 show z_n, $z_{n+1/2}$, v_n, $v_{n+1/2}$, $a_{n+1/2}$, $\rho_{n+1/2}$, ρ_n, p_n^*, $p_n^@$, $p_n^\#$, T_n^*, $T_n^@$, $T_n^\#$, and $T_{n+1/2}^\$$ as functions of t. Uncertainties for each quantitity are plotted, as are the simulated values experienced during entry.

Both z_n and $z_{n+1/2}$ (Figures 6.20 and 6.21) are accurately derived and have uncertainties smaller than the size of the symbols. $v_{n+1/2}$ (Figure 6.23) is accurately derived and has small uncertainties. $a_{n+1/2}$ (Figure 6.24) is not very accurately derived and has large uncertainties. However, the peak is quite well identified and this bodes well for the one useful result of $T_n^\#$. $\rho_{n+1/2}$ (Figure 6.25) is accurately derived after $t = 45$ s. ρ_n (Figure 6.26) is accurately derived, with larger uncertainties, between $t = 45$ s and 65 s. p_n^* (Figure 6.27) is accurately derived with small uncertainties after $t = 45$ s. $p_n^@$ (Figure 6.28) has such large uncertainties as to be useless. $p_n^\#$ (Figure 6.29) is accurately derived with small uncertainties after $t = 45$ s. T_n^* (Figure 6.30) has uncertainties of about 100 K between $t = 45$ s and 65 s. The temperature values in this time range are clearly centred on the correct 200 K result, so averaging them would improve the temperature measurement at the cost of vertical resolution. $T_n^@$ (Figure 6.31) is useless. All values of $T_n^\#$ that appear in Figure 6.32 have small uncertainties. However, only the measurement closest to the peak in acceleration is correct. If that peak can be identified well, then $T_n^\#$ provides one correct temperature measurement with a small uncertainty. In this example, the peak is clear and the $T_{54s}^\#$ measurement of about 200 K is easily selected. By repeating this work for different noisy values of v, I find that the peak in acceleration is almost always clear enough to narrow down the useful $T_n^\#$ measurement to at most two possibilities. $T_{n+1/2}^\$$ (Figure 6.33) has uncertainties

of less than 100 K between $t = 45$ s and 65 s. The temperature values in this time range are clearly centred on the correct 200 K result, so averaging them would improve the temperature measurement at the cost of vertical resolution.

The spacecraft's position as a function of time can be derived quite well using the techniques presented here. Correct values of atmospheric densities and pressures after 45 s (below 30 km) can be accurately derived with small uncertainties. Atmospheric temperatures can be accurately measured at the point of peak acceleration if that peak can be accurately identified. $T^{\$}_{n+1/2}$ is the most useful of the other techniques for measuring temperature. By reformulating the problem to eliminate poorly-constrained differences in speed, the uncertainties are reduced.

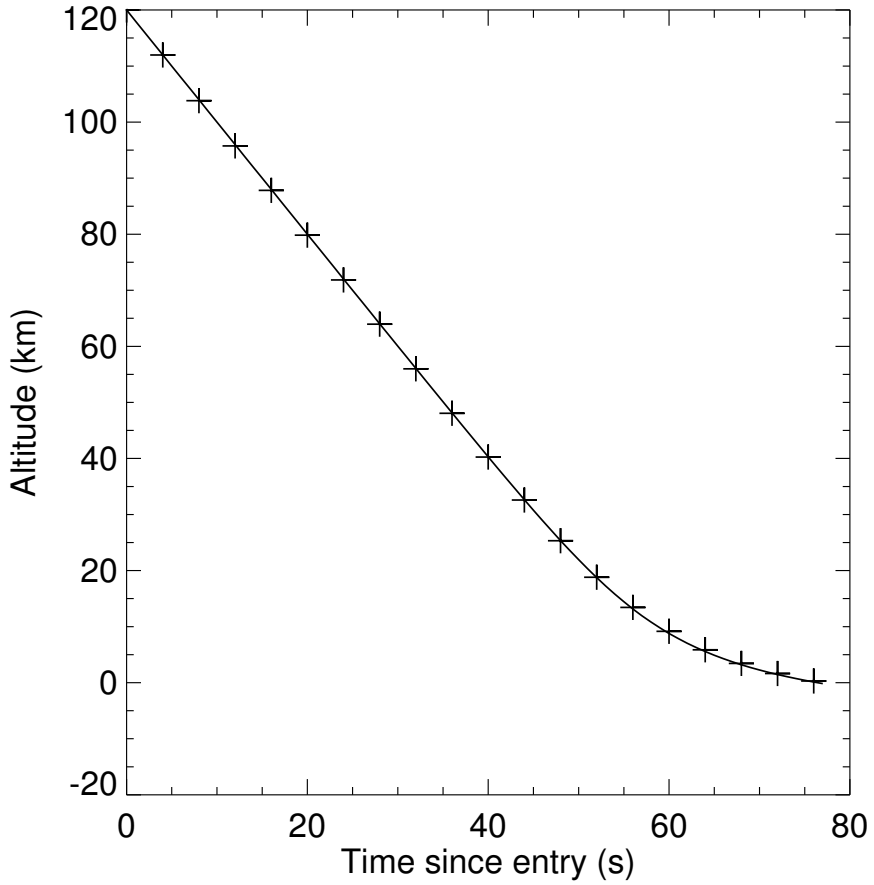

Figure 6.20: z_n (crosses) and σ_{z_n} (vertical lines) versus time calculated using noisy v. Continuous curve is simulated z versus t experienced during the atmospheric entry.

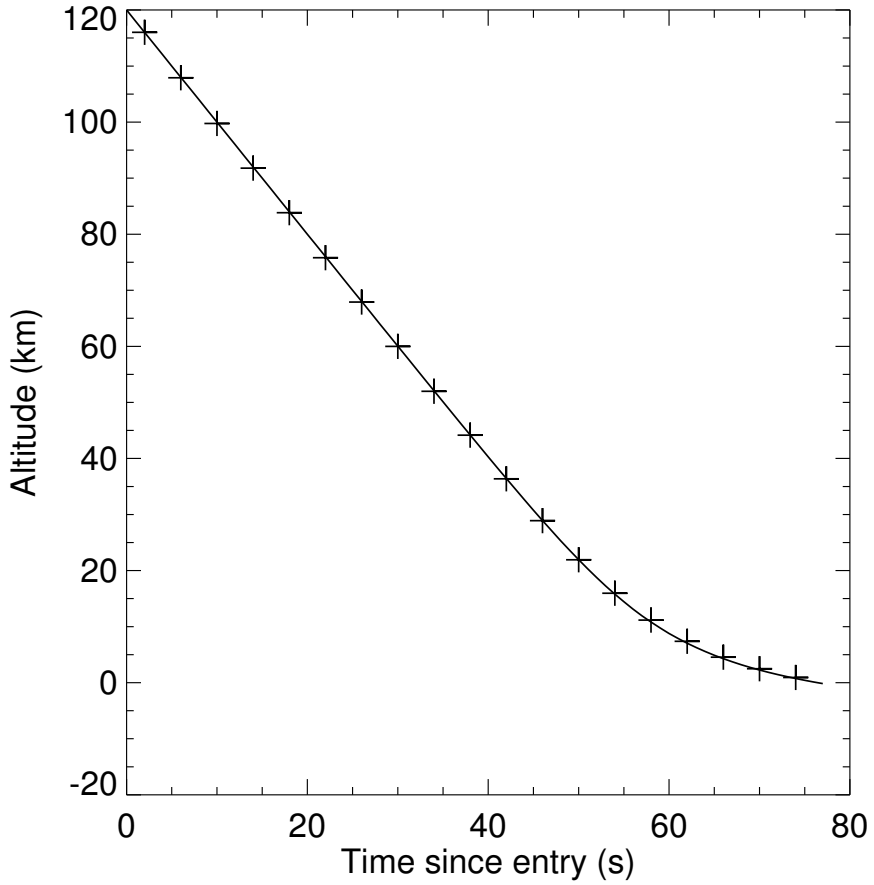

Figure 6.21: $z_{n+1/2}$ (crosses) and $\sigma_{z_{n+1/2}}$ (vertical lines) versus time calculated using noisy v. Continuous curve is simulated z versus t experienced during the atmospheric entry.

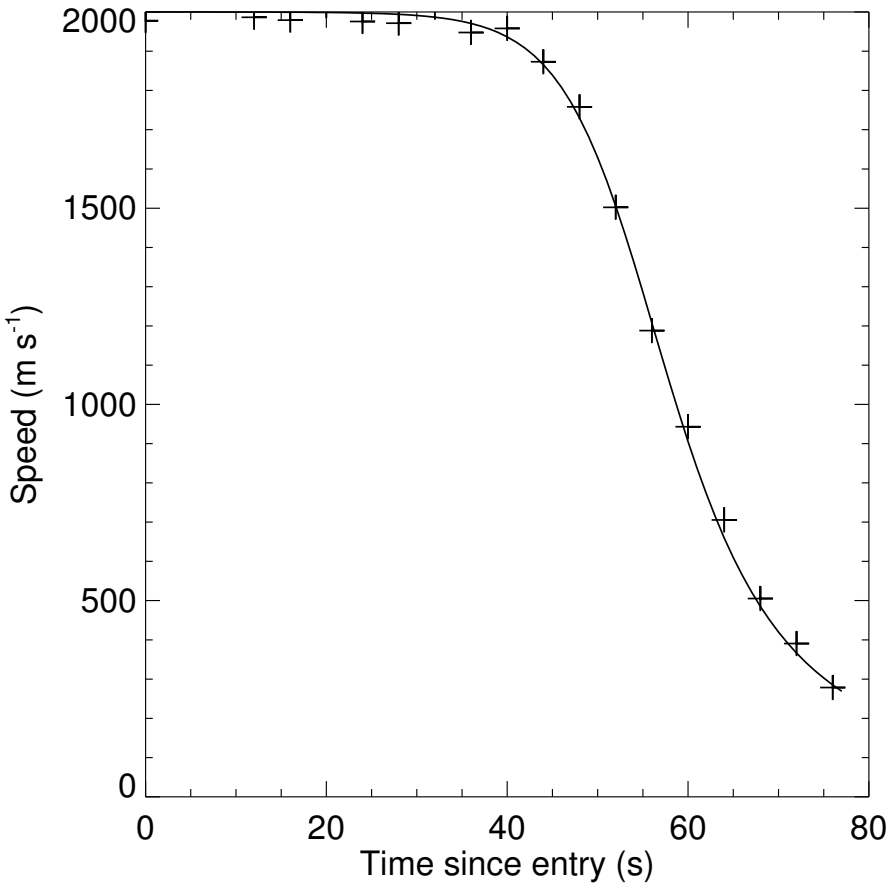

Figure 6.22: v_n (crosses) and σ_{v_n} (vertical lines) versus time calculated using noisy v. Continuous curve is simulated v versus t experienced during the atmospheric entry.

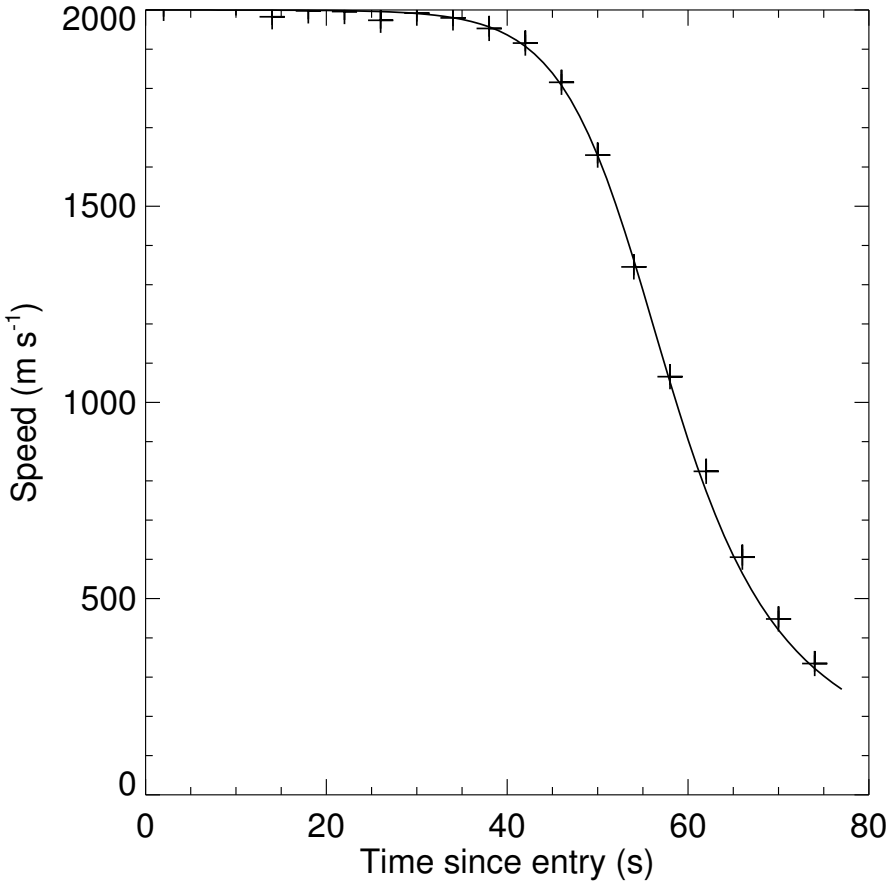

Figure 6.23: $v_{n+1/2}$ (crosses) and $\sigma_{v_{n+1/2}}$ (vertical lines) versus time calculated using noisy v. Continuous curve is simulated v versus t experienced during the atmospheric entry.

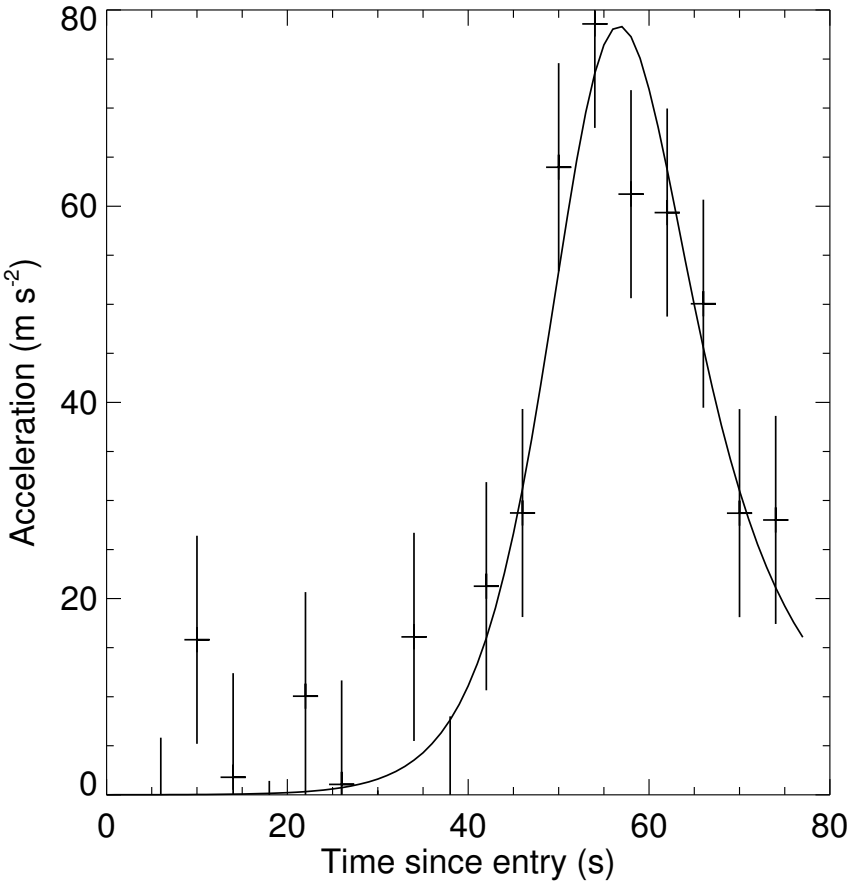

Figure 6.24: $a_{n+1/2}$ (crosses) and $\sigma_{a_{n+1/2}}$ (vertical lines) versus time calculated using noisy v. Continuous curve is simulated a versus t experienced during the atmospheric entry.

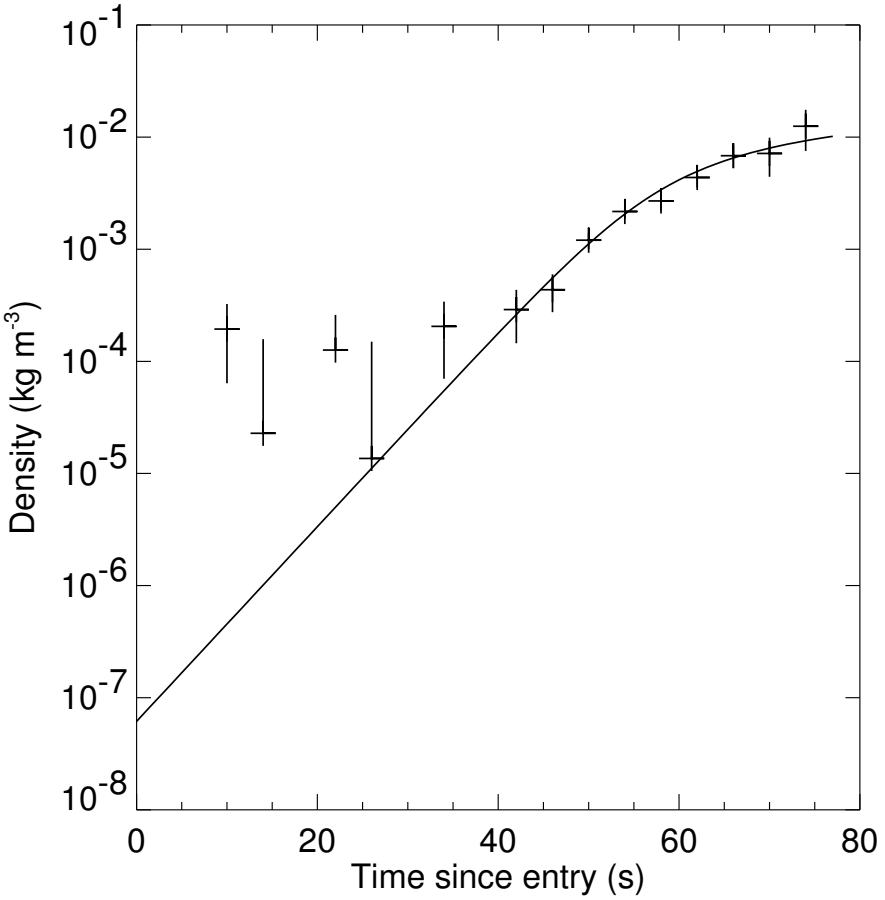

Figure 6.25: $\rho_{n+1/2}$ (crosses) and $\sigma_{\rho_{n+1/2}}$ (vertical lines) versus time calculated using noisy v. If $\rho_{n+1/2} - \sigma_{\rho_{n+1/2}}$ is negative, then only one side of the error bar is plotted. Continuous curve is simulated ρ versus t experienced during the atmospheric entry.

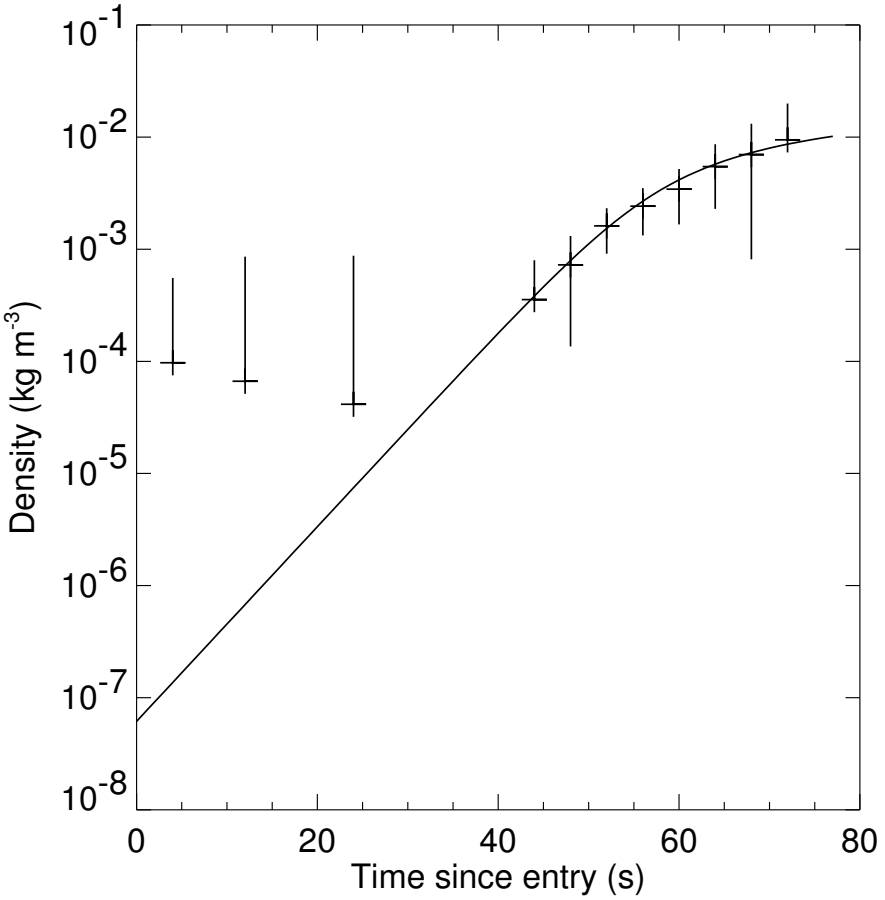

Figure 6.26: ρ_n (crosses) and σ_{ρ_n} (vertical lines) versus time calculated using noisy v. If $\rho_n - \sigma_{\rho_n}$ is negative, then only one side of the error bar is plotted. Continuous curve is simulated ρ versus t experienced during the atmospheric entry.

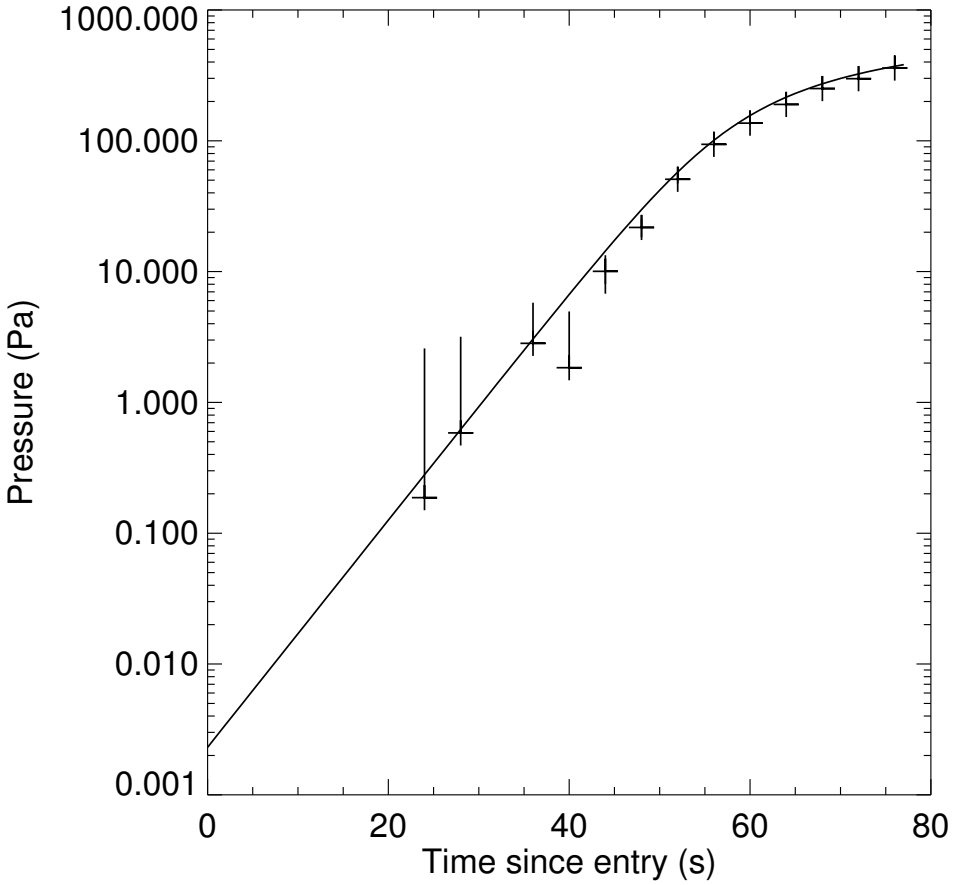

Figure 6.27: p_n^* (crosses) and $\sigma_{p_n^*}$ (vertical lines) versus time calculated using noisy v. If $p_n^* - \sigma_{p_n^*}$ is negative, then only one side of the error bar is plotted. Continuous curve is simulated p versus t experienced during the atmospheric entry.

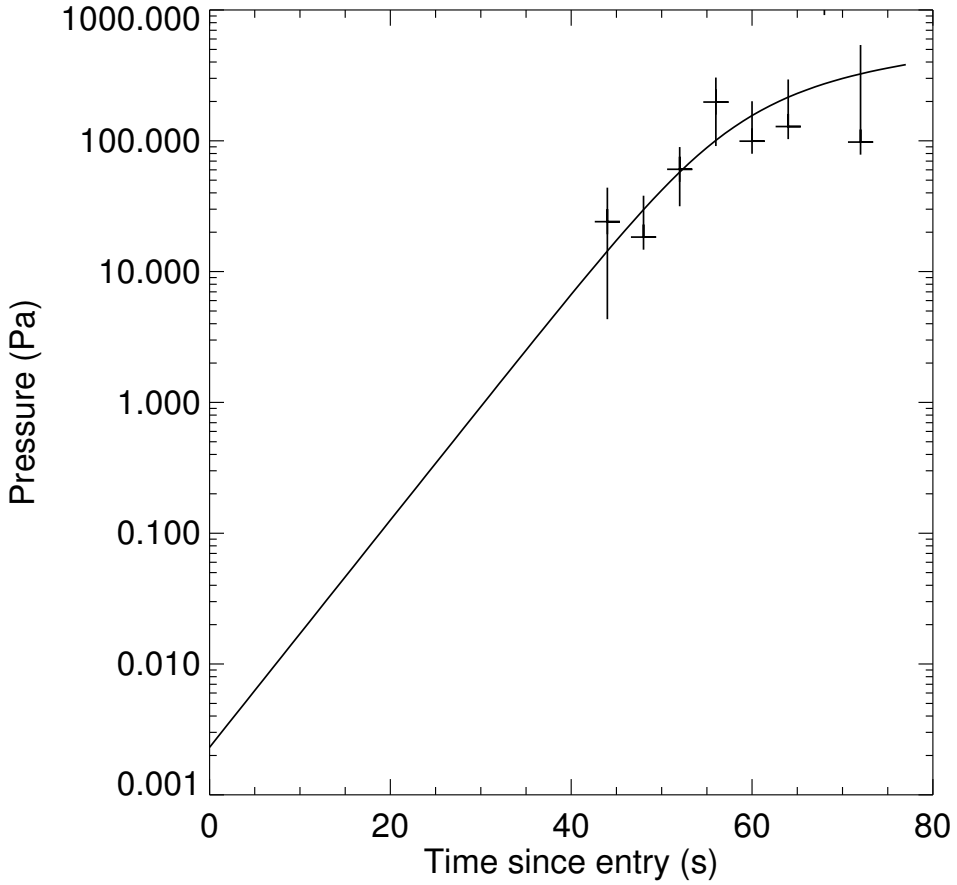

Figure 6.28: $p_n^{@}$ (crosses) and $\sigma_{p_n^{@}}$ (vertical lines) versus time calculated using noisy v. If $p_n^{@} - \sigma_{p_n^{@}}$ is negative, then only one side of the error bar is plotted. Continuous curve is simulated p versus t experienced during the atmospheric entry.

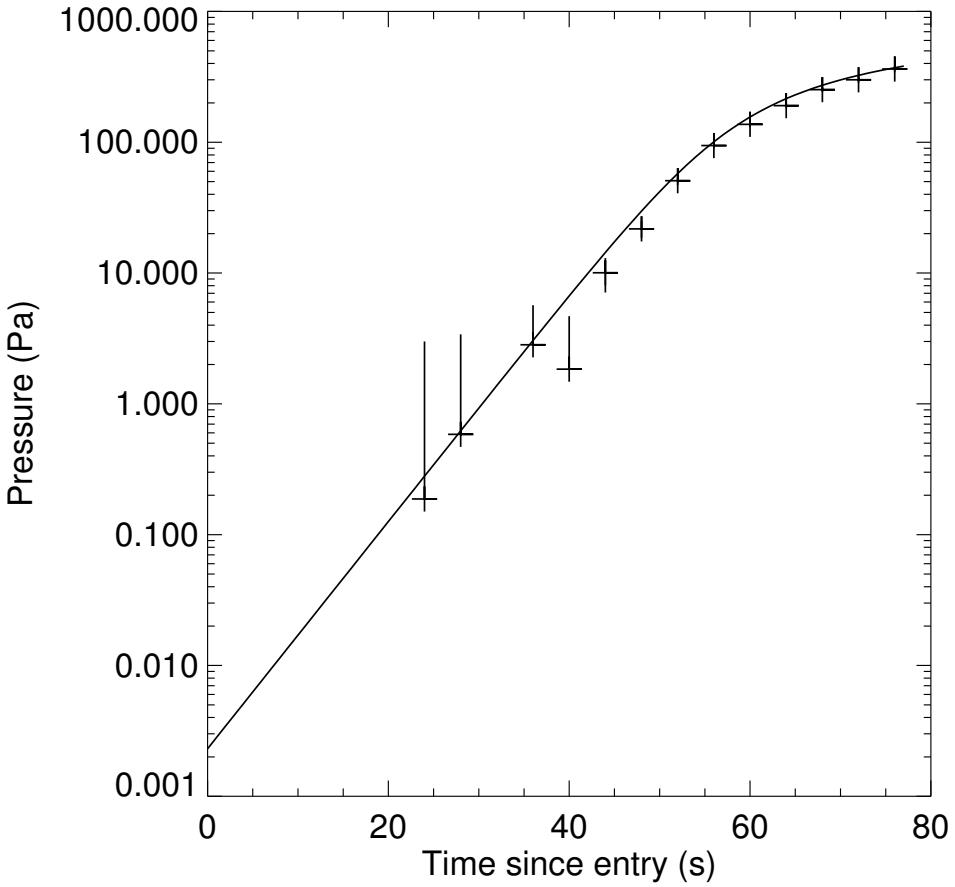

Figure 6.29: $p_n^{\#}$ (crosses) and $\sigma_{p_n^{\#}}$ (vertical lines) versus time calculated using noisy v. If $p_n^{\#} - \sigma_{p_n^{\#}}$ is negative, then only one side of the error bar is plotted. Continuous curve is simulated p versus t experienced during the atmospheric entry.

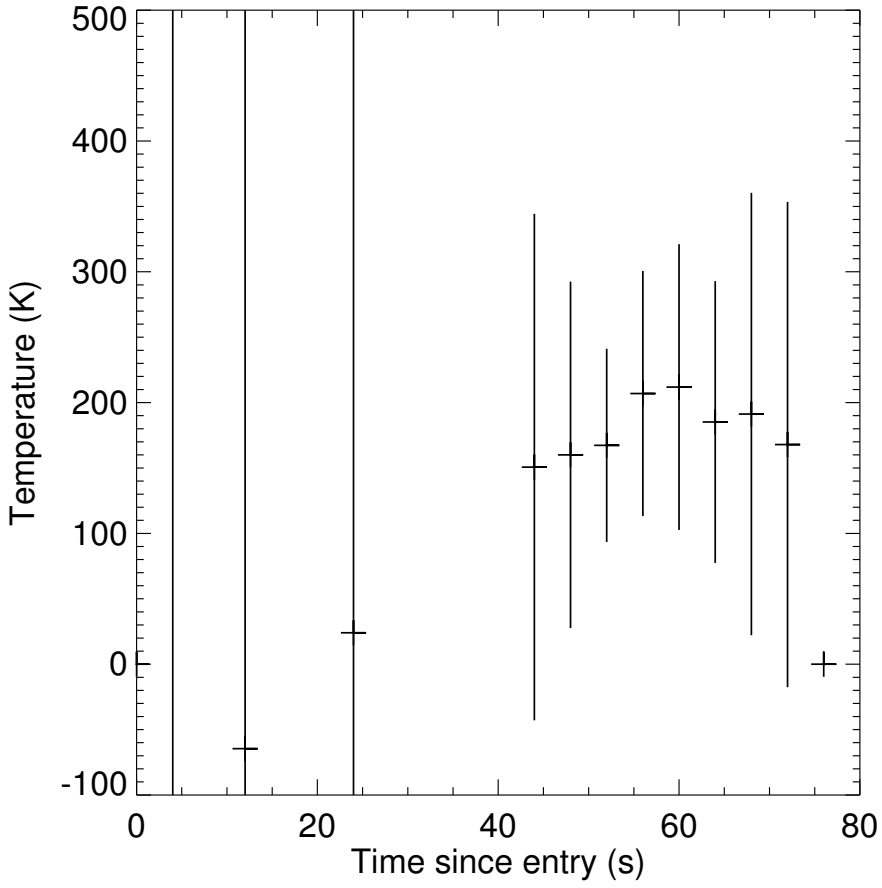

Figure 6.30: T_n^* (crosses) and $\sigma_{T_n^*}$ (vertical lines) versus time calculated using noisy v. Simulated T during the atmospheric entry is 200 K.

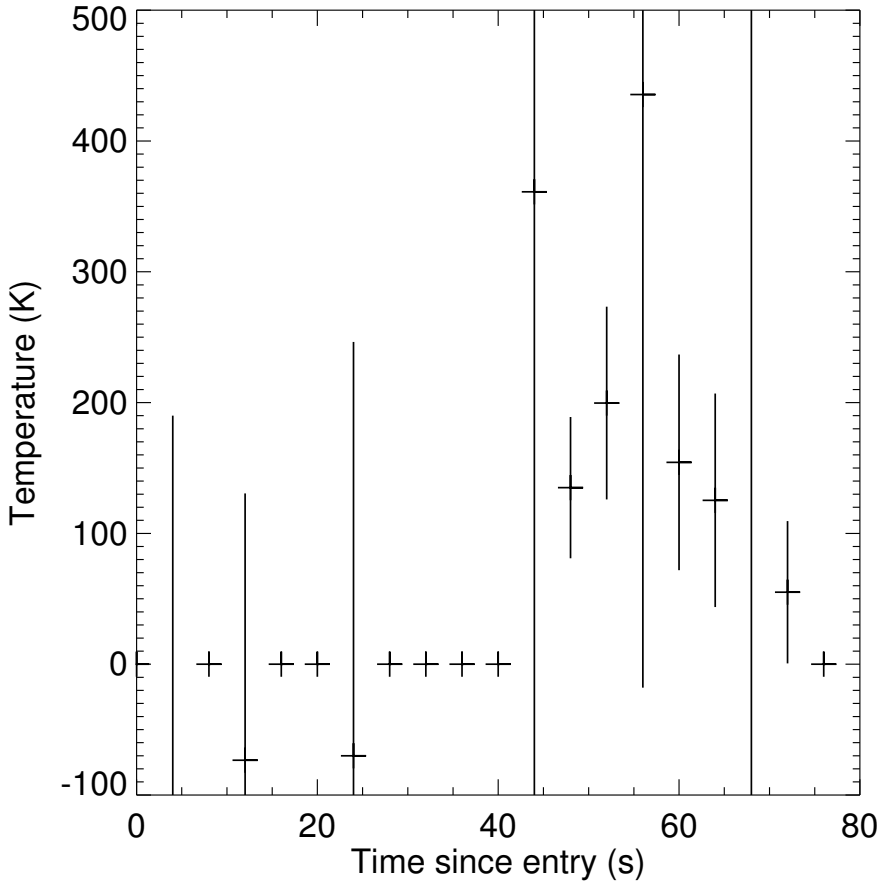

Figure 6.31: $T_n^{@}$ (crosses) and $\sigma_{T_n^{@}}$ (vertical lines) versus time calculated using noisy v. Simulated T during the atmospheric entry is 200 K.

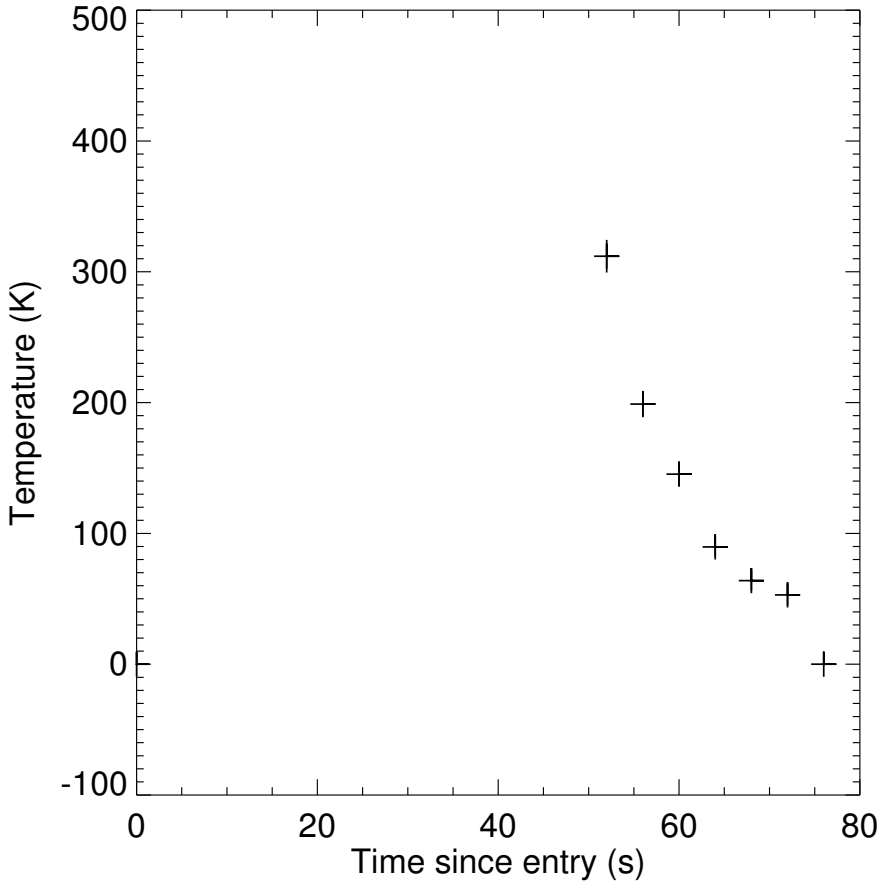

Figure 6.32: $T_n^{\#}$ (crosses) and $\sigma_{T_n^{\#}}$ (vertical lines) versus time calculated using noisy v. Simulated T during the atmospheric entry is 200 K.

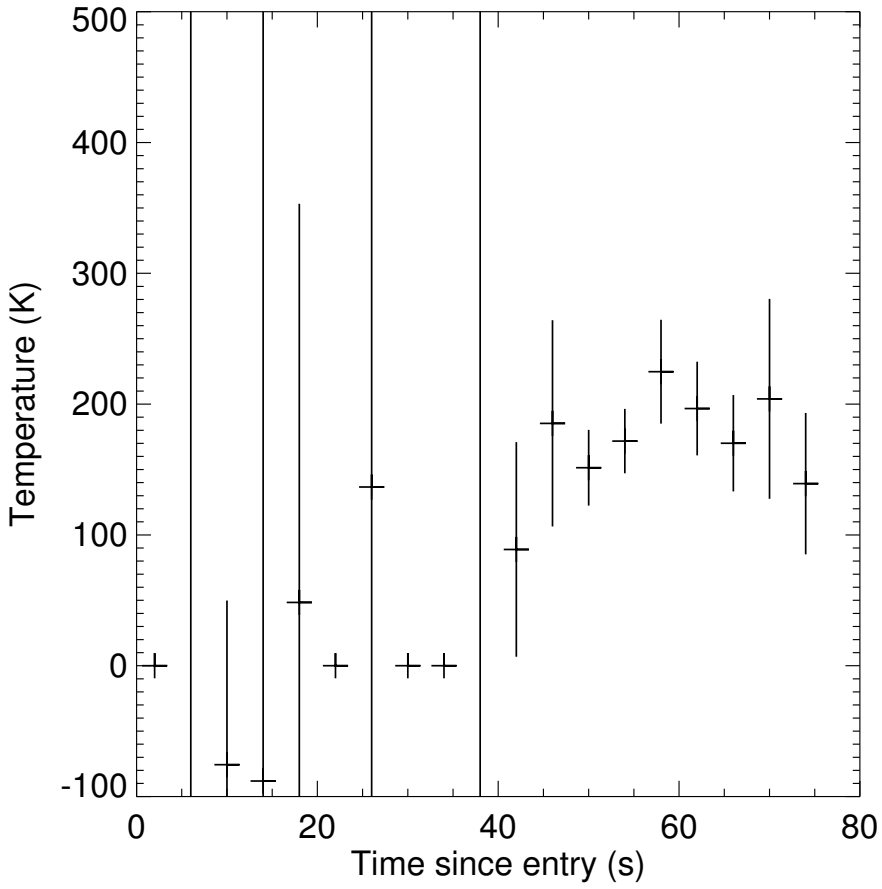

Figure 6.33: $T^{\$}_{n+1/2}$ (crosses) and $\sigma_{T^{\$}_{n+1/2}}$ (vertical lines) versus time calculated using noisy v. Simulated T during the atmospheric entry is 200 K.

6.8 Conclusions

Several different techniques for measuring atmospheric properties during entry from telemetry have been compared. Some, such as p^*, $p^\#$, T^*, $T^\#$, and $T^\$$, appear useful. When trying to measure and analyse small changes in noisy data, it is clear that great care must be taken to select the best approach.

Two assumptions that I have made deserve further discussion. Firstly, I have assumed that the measured v are dominated by random noise when they are actually dominated by systematic errors due to the transmitter being very sensitive to acceleration. Uncertainties in derived quantities are not too greatly affected by this, but the values of the derived quantities are. Small differences in speed, which are interpreted as accelerations, could be dominated by frequency drift. The $T^\$$ technique is least affected by this. To quantify whether this renders some of my techniques useless, I would have to see how a prescribed frequency drift affects my calculations of z, a, ρ, p, and T. Secondly, I have often assumed a constant value of C_D. In Chapter 5 I have shown that this assumption is useful. Where I have calculated densities or pressures using this assumption, an extra uncertainty of 25% should be incorporated. Where I have calculated temperatures using this assumption, the extra uncertainty is much smaller ($\sim 10\%$).

My simplified geometry and neglect of gravity on the spacecraft's trajectory are useful for describing the techniques, but are not difficult to incorporate into a real analysis tool. How useful might these techniques be in practice? Clearly this work can be performed much more accurately using onboard accelerometers, but these techniques should give reasonable trajectories. The derived atmospheric properties have such large uncertainties that they are only likely to be useful either if the planet's atmosphere has not been well studied before or if there is public or political interest in poor quality results from an otherwise failed mission. An over-riding problem is the separation of changes in frequency due to drift and due to the Doppler shift. Time intervals may need to be increased such that the change in frequency

due to the change in speed during the extended time interval is comfortably greater than the likely drift in frequency.